# A Multiple Level-Set Approach for Modeling Unconstrained Solidification

Hasan Shetabivash

A Thesis
In the Department
of
Mechanical, Industrial and Aerospace Engineering

Presented in Partial Fulfillment of the Requirements
For the Degree of
Doctor of Philosophy (Mechanical Engineering) at
Concordia University
Montreal, Quebec, Canada

November 2018

**CONCORDIA UNIVERSITY**

**SCHOOL OF GRADUATE STUDIES**

This is to certify that the thesis prepared

By: Hasan Shetabivash

Entitled: A Multiple Level-Set Approach for Modeling Unconstrained Solidification

and submitted in partial fulfillment of the requirements for the degree of

Doctor Of Philosophy (Mechanical Engineering)

complies with the regulations of the University and meets the accepted standards with respect to originality and quality.

Signed by the final examining committee:

_____Chair
Dr. Luis Amador

_____ External Examiner
Dr. Mehdi Raessi

_____ External to Program
Dr. Attila Michael Zsaki

_____ Examiner
Dr. Christian Moreau

_____ Examiner
Dr. Brian Vermeire

_____Thesis Co-Supervisor
Dr. Ali Dolatabadi

_____Thesis Co-Supervisor
Dr. Marius Paraschivoiu

Approved by _____
Dr. Ali Dolatabadi, Graduate Program Director

January 11, 2019 _____
Dr. Amir Asif, Dean
Gina Cody School of Engineering and Computer Science

# Abstract

## A Multiple Level-Set Approach for Modeling Unconstrained Solidification

**Hasan Shetabivash, PhD**

**Concordia University, 2018**

This thesis focuses on numerical simulation of the freezing process of liquid droplets on cold substrates. Solidification of droplets is one of the most challenging phenomenon for numerical modelling since various complicated physical mechanisms are involved. Dealing with the jump conditions at interfaces has been a long-term concern in numerical simulations. Moreover, the tri-junction point where three-phases come into contact requires special treatment. Furthermore, density expansion during freezing process should be taken into account.

In this thesis, we propose a level-set based model to represent three-phase solidification physics. Liquid and solid interfaces are represented by two different level-sets in order to deal with the phases separately. The liquid-gas interface is advected under an external velocity field obtained from solving Navier-Stokes equations. The solid-liquid level-set, on the other hand, evolves according to the freezing rate of the liquid. The level-set associated with the solid-liquid interface is comprised of two segments: active, and passive. The active part of the level-set evolves based on temperature gradients and latent heat of fusion. While, the passive part is merely utilized for imposing the angle at the tri-junction point. We solve a Hamilton-Jacobi type equation in the passive part of the liquid-solid interface to impose a constant or variable angle at the tri-junction point.

Furthermore, to consider the effect of density expansion, we added a source term into the continuity equation. The source term induces velocity in the domain by which the liquid-gas interface evolves. Moreover, a source term is added to the level-set advection equation to impose mass conservation in the liquid phase. The effect of density variation is included in the energy equation as well.

The proposed numerical approach is validated using benchmark problems. In addition, we compared numerical results of water droplet freezing on a cold substrate with experimental results available in the literature. Through the comparison, we prove that the proposed model is capable of accurately predicting solidification behavior.

# Acknowledgements

I would like to express my sincere gratitude to my supervisors, Prof. Ali Dolatabadi and Prof. Marius Paraschivoiu for their continuous support of my PhD study; without their motivation, knowledge, insightful comments, encouragement and hard questions that triggered several innovative solutions during the process of researching and writing the thesis, this accomplishment would not have occurred.

I would like to gratefully acknowledge the funding provided by NSERC, CARIC, and Horizon 2020 for the PHOBIC2ICE project by which this research is supported.

I am also grateful of my fellow lab-mates for the stimulating discussions and the laughter moments which decreased the pressure of hard work. I would like to thank my friends for expecting nothing less than triumph from me during my Ph.D. program.

# Table of Contents

# List of Figures

# List of Tables

# Nomenclature

| | |
|---|---|
| $A$ | Area |
| $C$ | Heat capacity |
| $C_{app}$ | Apparent heat capacity |
| $C_{eff}$ | Effective heat capacity |
| $\mathbf{F}_b$ | Body force |
| $H$ | Enthalpy |
| $k$ | Thermal conductivity |
| $\hat{L}_H$ | Apparent latent heat of fusion |
| $L_H$ | Latent heat of fusion |
| $P$ | Pressure |
| $S_t$ | Thermal source term |
| $T$ | Temperature |
| $t$ | Time |
| $\mathbf{u}$ | Velocity |
| $V$ | Volume |
| $v_n$ | Normal velocity |

**Dimensionless Numbers**

| | |
|---|---|
| $Bo$ | Bond number |
| $Pr$ | Prandtl number |

$S$ Dimensionless droplet height

$St$ Stefan number

$U_r$ Dimensionless velocity

$We$ Weber number

**Greek Symbols**

$\Gamma$ Interface

$\mu$ Dynamic viscosity

$\Omega$ Domain

$\phi$ Liquid interface

$\psi$ Solid interface

$\rho$ Density

$\sigma$ Surface tension

$\tau$ Dimensionless time

$\Theta$ Dimensionless temperature

**Subscriptions**

$f$ Face

$l$ Liquid

$s$ Solid

# Chapter 1

# Introduction

## 1.1 Background and Motivation

There are applications of water droplet solidification on solid surfaces in various industries (Fig. 1.1). For instance, snow or freezing rain may lead to formation of slush, or clear ice on aircraft critical surfaces. Even in ambient conditions above freezing temperatures, ice can be formed as a result of existence of fuel in the fuel tanks which is below freezing temperature. Moreover, droplets in clouds usually reach to high altitudes where super-cooling occurs. In this conditions, droplets may become extremely super-cooled to around $-40^oC$. Airplanes flying in this altitudes, are at risk of having ice accumulated on their critical surfaces, as result of impact and immediate freezing of super-cooled droplets (Bragg [1]).

Ice accumulation on critical parts of an airplane (e.g. wings, tail, and stabilizers) degrades its overall aerodynamic behavior. Even small changes in the aerodynamics of the airplane could cause significant reduction of stability, maximum lifting capability, control surface effectiveness, and engine performance. Having considered aforementioned risks caused by ice formation on aircraft surfaces, evaluation of anti-icing capabilities performed by advanced freezing tests is essential in the aerospace industry.

Deposition of ice on the turbine blades and tower, operating in cold weather conditions is one of the most critical issues in the wind turbine industry. Efficiency of turbines may be degraded as a result of formation of ice layer and subsequent alteration of blades profile shape. Even a thin layer of ice on wind turbine blades undermines their aerodynamic performance and hence power generation would be reduced considerably. In addition, increase of maintenance costs, structural failure, fatigue of blades are another results of ice accretion on turbine blades. Furthermore, ice can be detached and thrown from rotating blades posing catastrophic safety issues, especially at the vicinity of public roads, power lines, and shipping routes.

Figure 1.1: Ice accumulation on critical parts of airplane and wind turbines

Another application of solidifying droplets is in thermal spraying industry. Surface treatment using plasma spraying is one of the most promising methods for producing surfaces with special characteristics such as wear, corrosion, erosion and thermal shock resistance. In thermal spraying process fine particles are injected into plasma jet, while are melted and thrown on designated substrate to form a thin layer. Successive impingement of these molten particles builds up coating which provides the surface with special characteristics. The quality of coating and thermal properties of the coated surface is considerably correlated to the behavior of impinging droplets. Spreading and solidification of impinging droplets on the surface and subsequently buildup of splats on the substrates on top of each other will finally determine the quality and microstructure of the surface. Dynamics of deformation and solidification of particles, greatly affects the physical properties of the substrate such as surface roughness, porosity, and adhesion strength of coating.

## 1.2 Dimensionless Parameters

Several non-dimensional numbers can be utilized to establish major parameters describing solidification physics and to enable direct comparison between various cases. We use these parameters to characterize the heat transfer and fluid flow (Vu et al. [2]).

Since heat transfer is the principal mechanism in droplet solidification we use liquid thermal properties to scale the time.

$$\tau_r = \frac{\rho_l C_{Pl} D_0^2}{k_l}, \quad \tau = \frac{t}{\tau_r}, \tag{1.1}$$

where $\rho_l$, $C_{Pl}$, $k_l$ are liquid density, liquid specific heat and liquid heat conductivity, respectively. Hence the dimensionless number representing time would be the ratio of time to the characteristic time. As a scale for velocity we use the ratio of length scale which is droplet diameter to the time scale.

$$U_r = \frac{D_0}{\tau_r}, \tag{1.2}$$

and we use the following dimensionless temperature

$$\Theta = \frac{T - T_c}{T_m - T_c}. \tag{1.3}$$

One of the major parameters governing the droplet freezing process is Prandtl number which is the ratio of momentum diffusivity to thermal diffusivity.

$$Pr = \frac{C_{Pl}\mu_l}{k_l}. \tag{1.4}$$

Where $\mu_l$ represents the viscosity of the liquid. The rate of solidification can be characterized with the Stefan number which is the ratio of sensible heat to latent heat.

$$St = \frac{C_{Pl}\,(T_m - T_c)}{L_H} \tag{1.5}$$

Where $L_H$ represents the latent heat of fusion. The ratio of inertial to the surface tension forces are represented by Weber number,

$$We = \frac{\rho_l U^2 D_0}{\sigma}. \tag{1.6}$$

Where $U$ represents the magnitude of velocity and $\sigma$ is the surface tension. Taking into account the effects of gravity, the dimensionless parameter related to gravity and surface tension forces is Bond number

$$Bo = \frac{\rho_l g D_0^2}{\sigma} \tag{1.7}$$

representing the ratio of gravity to surface tension forces.

## 1.3 Experiments on Droplet Solidification

This section is dedicated to experimental studies investigating droplet impact and subsequent solidification process. Overall procedure of droplet impact and solidification can be divided into two distinct phases; Spreading of the droplet on the surface; Solidification of droplet. After droplet impacts on the surface, depending on the characteristics

of the liquid and the substrate, droplet spreads on the surface. Afterwards, solidification of the droplet will be initiated and it takes some time for droplet to completely freeze. The influence of these mechanisms on each other, was investigated experimentally by Madejski [3], who postulated that spreading diameter of droplet is almost independent on the thermal properties of the surface. Bennett and Poulikakos [4] conducted a combined theoretical and experimental study in order to investigate influential parameters in heat transfer of solidifying metal droplet. They represented that thermal conductivity of substrate significantly affects cooling process of the droplet. Performing various experiments, they concluded that thermal conductivity of the substrate can markedly affect the grain size of solidified splat.

Kang et al. [5] provided experimental results on subsequent impingement of two droplets on a substrate indicating that cooling rate at the bottom of the droplet which is in contact with the substrate is markedly higher. In addition, they postulated that contact resistance at splat substrate and at the interface of two splats significantly affects the solidification process. Performing experimental studies alongside numerical results, Pasandideh-Fard et al. [6] concluded that influence of solidification process on droplet impact dynamics can be neglected for $\sqrt{St/Pr} << 1$.

Fukumoto and Huang [7], based on experimental results, concluded that transition from splash to disk shape spreading will occur by increasing temperature of the substrate. Besides, experimental results yielded that solidification rate at the interface between splat and the substrate is higher than inner region of the splat, in the case of low temperature substrate. Regarding effect of substrate temperature on the spreading dynamic they postulated that flattening rate of droplet on surfaces with high temperatures are greater. An experimental research focused on impingement of molten particles on aluminum surface, performed by Bhola and Chandra [8], revealed that solidification process could hardly affect the dynamics of impact. Besides, they found that reducing substrate temperature may stimulate droplet break up. Attinger et al. [9] used surfaces with various temperatures to investigate influence of spreading and solidification on each other. Based on the results, solidification time is dependent on the substrate temperature. In addition, substrate temperature markedly influences spreading process for $St$ ranging from 0.77 to 0.48. However, at high temperatures spreading factor is essentially independent of the substrate temperature.

Various experimental studies attempted to investigate liquid droplet solidification and its characteristics. For instance, Hindmarsh et al. [10] performed experimental study and provided different stages of droplet solidification. Wang et al. [11] experimentally investigated water droplet solidification with the focus on morphology and shape of freezing during solidification. They reported that droplet shape changes while solidifying and grows in the direction perpendicular to the surface. In order to quantify the morphological changes of droplet during freezing, they used deformation factor as

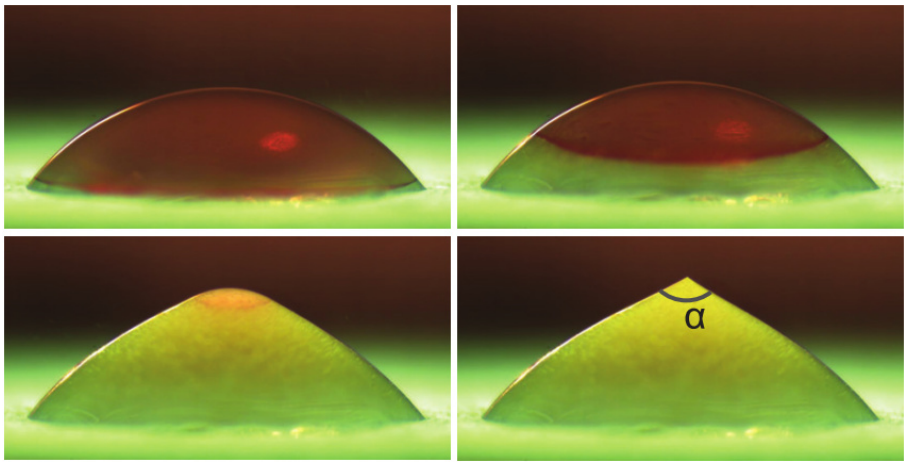


Figure 1.2: Freezing process of a droplet under constant surface temperature (Marin et al. [12])

following:

$$S = \frac{H}{H_i}.$$

Where, $H$, and $H_i$ are instantaneous and initial height of the droplet, respectively. They reported that deformation factor of water droplet is about 1.15-1.2 after complete solidification process. Based on reported results, droplet freezing starts when the temperature of substrate is cooled far enough below the freezing point of water and freezing front starts from the surface and moves to the top of the liquid droplet. At the final steps of solidification, a protrusion which is a result of density difference between ice and water is formed at the top of the droplet which gives the droplet a peach shape. Several techniques have been used by researchers to study droplet morphology change during solidification. Jin et al. [13] used LIF method to visualize the freezing process of small droplets. Hu and Jin [14] used a novel lifetime-based molecular tagging thermometry (MTT) technique to experimentally investigate droplet solidification process. Based on the detailed spatially and temporally resolved temperature distribution measurements they found that the temperature of liquid part of the droplet increases while the solidifying interface moves upward. They proposed that the increase in the liquid temperature is a result of latent heat release at the solidification line. Marin et al. [12] experimentally studied the droplet solidification process in a Hele-Shaw geometry. They suggested that the cone angle at top of the droplet is independent of substrate temperature and wetting angle of the droplet.

Effect of hydrophobicity of the surface on freezing of the droplet is an area which attracts attention of many researchers during the last decade. The substantial strategies to form hydrophobic or super-hydrophobic surfaces is roughening of a hydrophilic surface or alteration of the surface chemistry using low surface energy materials. There

are two different models to describe behavior of droplet on textured hydrophobic surfaces: Wenzel; Cassie Baxter. In the former state droplet conforms to the contour of textured surface and in the latter regime droplet rests on the surface, over the trapped air in the cavities. Tourkine et al. [15] used experimental approach to investigate effect of Cassie-Baxter state hydrophobicity on icing of water droplet. Based on their results, hydrophobicity of the surface delays the freezing process by a factor of 3 and 5 which is mainly caused by trapped film of air which hinders the heat transfer to the substrate. Moreover, Singh and Singh [16] investigated effect of non-columnar thin film on freezing process, by performing an experimental study on Ag non-columnar thin film samples. Their results unveiled that the non-columnar film significantly hinders the freezing rate mainly because of reduced effective liquid-solid interface area.

Effect of hydrophobicity on the freezing of water droplet further investigated by Huang et al. [17] by comparing freezing of droplet on various surfaces with different contact angles. They fabricated super-hydrophobic surfaces by etching and fluorinating modification method and the $156^{o}$ was the largest obtained contact angle. The experimental results, divulged that contact angle directly affects the freezing of droplet and alters the crystal formation and growth. They postulated that freezing process initiated later because of smaller contact area between the droplet and the surface. They also reported formation of protrusion on the top of the droplet and they related this phenomenon to density change of water and the dissolved air discharge in water.

Most of the studies regarding water droplet solidification focused on the effect of substrate properties, such as super-hydrophobicity, on the freezing process neglecting the effect of surrounding gas characteristics. Jung et al. [18], performed an experimental study to investigate how shear gas flow can alter freezing of super-cooled droplet mechanism. Ice-phobicity of the surface can become ineffective by some changes in environmental conditions. Based on their results, crystallization of super-cooled droplets can be initiated at the interface of droplet and gas because of evaporative cooling. By subjecting super-cooled sessile water droplet to nitrogen shear flow with various humidity, they showed that crystallization is initiated by homogeneous nucleation near the gas-liquid interface. Chaudhary and Li [19] confirmed delayed freezing process of water droplet on hydrophobic surfaces by carrying out experiments on various hydrophilic and hydrophobic surfaces.

## 1.4 Numerical Methods for Modelling Solidification

Due to the fast paced progress in computer hardware and software technologies, numerical simulations have become attractive for investigation of flows with free surfaces as a complement of experimental studies. However, in spite of decades

of continuous research the numerical simulations of free-surface flows are still far away from being an efficient approach for studying complicated multiphase physical phenomenon. The major challenges include, but not limited to, the accurate time and space tracking of the free surface, the existence of high density ratios within the flow field, and the accurate calculation of the surface tension forces. Complexities associated with the numerical simulation of droplet solidification are because various physical processes should be taken into account. From fluid flow point of view, appropriate methodologies are needed to track the interface between the liquid and the gas. In addition, growth of the liquid-solid interface, heat transfer, and phase change during solidification need special treatment. Generally, available methods for treating the solidification of liquids can be categorized into four distinct groups namely; enthalpy, front tracking, phase field, and level-set. The details of these methods will be discussed in this section.

### 1.4.1 The Enthalpy Method

Enthalpy method, proposed by Voller [20] has been extensively used for numerical simulation of solidification of liquids. In this method, an indicator function, which ranges from zero to one, is introduced to track the volumes of different phases. Each phase can be distinguished based on the values of the indicator function. At the interface, however, the indicator function is discontinuous. General form of the energy equation based on the total enthalpy, can be written in the following form,

$$\frac{\partial \rho H}{\partial t} + \nabla \cdot (\rho \mathbf{u} H) = \nabla \cdot (k \nabla T)\,. \tag{1.8}$$

Where $\rho$, and $H$ represent the density and enthalpy. Note that properties of materials are calculated by weighted averaging based on the indicator function. This equation can be discretized and solved like other diffusion equations with available discretization schemes and methods. However, in the presence of solidification treating the solidification front is problematic because there is a we need to include release of latent heat of fusion at the solidifying front. There are several approaches to include latent heat of fusion in the energy equation which are represented in the following sections.

#### Apparent Capacity Method

In this method which is proposed by Hashemi and Sliepcevich [21] an apparent thermal capacity is defined in such a way that includes the latent heat of fusion. Apparent capacity is defined in the range of phase change temperatures to consider the latent heat as well as the sensible heat at the liquid-solid interface. Apparent capacity for

uniformly released latent heat at the liquid-solid interface can be defined as follows,

$$C_{app} = \frac{\int_{T_s}^{T_l} C(T)dT + L_H}{T_l - T_s}, \tag{1.9}$$

where $T_s$, $T_l$, $T$ and $C(T)$ indicate solid temperature, liquid temperature, temperature, and specific capacity as a function of temperature, respectively. Using this method the energy equation can be simplified and written based on temperature as a single variable.

$$\frac{\partial \rho C_{app} T}{\partial t} + \nabla \cdot \left(\rho C_{app} \mathbf{u} T\right) = \nabla \cdot \left(k \nabla T\right). \tag{1.10}$$

Where $\rho$ represents the density. Apparent specific heat can be calculated either explicitly or implicitly. In the explicit scheme, the apparent capacity is calculated from previous temperature in the computational domain. Using implicit scheme the capacity is evaluated from current field of temperature. Despite the simplicity of this method, it has a problem in dealing with nodes that their temperature falls from above the liquidus temperature to below the solidus temperature. As a result, heat of fusion would not be accounted in those cells.

**Effective Capacity Method**

Effective capacity method (Poirier and Salcudean [22]) is an extension of the apparent capacity method which can be evaluated by integrating apparent capacity over the control volume.

$$C_{eff} = \frac{\int C(T)_{app} dV}{V}, \tag{1.11}$$

where, $V$ is the volume of the control volume, and $C(T)_{app}$ is the apparent heat capacity. For the cases with steep temperature gradients at the interface like what happens in solidification of water, this method will be considerably expensive. Because higher sampling frequencies are required during the numerical integration (Poirier and Salcudean [22]). Using this method, final form of energy equation can be written as following,

$$\frac{\partial \rho C_{eff} T}{\partial t} + \nabla \cdot \left(\rho C_{eff} \mathbf{u} T\right) = \nabla \cdot \left(k \nabla T\right), \tag{1.12}$$

**Source Based Method**

Source based method is presented by Voller and Cross [23]. In this method the enthalpy is expressed as a function of temperature,

$$H = C_P T + \Delta H, \tag{1.13}$$

where $\Delta H$ is the heat of fusion during solidification process. Substituting this relation into Eq. 1.8 yields,

$$\frac{\partial \rho \left(C_P T + \Delta H\right)}{\partial t} + \nabla \cdot \left(\rho \mathbf{u} \left(C_P T + \Delta H\right)\right) = \nabla \cdot \left(k \nabla T\right), \tag{1.14}$$

$$\frac{\partial \rho C_P T}{\partial t} + \nabla \cdot \left(\rho \mathbf{u} C_P T\right) = \nabla \cdot \left(k \nabla T\right) + S_t, \tag{1.15}$$

where $S_t$ is source term which can be expressed as following,

$$S_t = -\left(\frac{\partial \rho \Delta H}{\partial t} + \nabla \cdot \left(\rho \mathbf{u} \Delta H\right)\right), \tag{1.16}$$

In order to calculate the source term, latent heat should be represented as a function of temperature. There are two approaches in the literature for expressing the latent enthalpy as a function of temperature. In the first approach the latent enthalpy is expressed directly as a function of temperature (Voller et al. [24]).

$$\Delta H = \begin{cases} 0 & T \leq T_{sol} \\ \frac{L}{2\delta}\left(T - \frac{T_{liq}+T_{sol}}{2} + \delta\right) & T_{sol} < T \leq T_{liq} \\ L & T > T_{liq} \end{cases} \tag{1.17}$$

where, $L_H$ is the latent heat of fusion, and $\delta = \frac{T_{liq}-Tsol}{2}$ is a temperature half range over which the phase change occurs. Using this function, source term in Eq. 1.15 is calculated implicitly or explicitly. The set back of this method is difficulty in calculation of solid fraction from calculated enthalpy of the domain. Another approach which is easier for implementation is expressing the enthalpy of fusion in terms of solid fraction.

$$\Delta H = C_p T + \gamma L_H. \tag{1.18}$$

Consequently, the source term in Eq. 1.15 can be calculated as follows,

$$S_t = -L_H \left(\frac{\partial \rho \gamma}{\partial t} + \nabla \cdot \left(\rho \mathbf{u} \gamma\right)\right), \tag{1.19}$$

where $\mathbf{u}$, $\gamma$ represent velocity and solid fraction, respectively. Various functions are proposed for evaluating solid fraction from temperature. For instance, a linear approximation of solid fraction as a function of time can be expressed as following,

$$\gamma = \begin{cases} 1 & T > T_{liq} \\ \frac{T-T_{sol}}{T_{liq}-T_{sol}+\epsilon} & T_{sol} < T < T_{liq} \\ 0 & T < T_{sol} \end{cases} \tag{1.20}$$

Alternatively, an error function expressed by Rösler and Brüggemann [25] can be used for evaluation solid fraction as following,

$$\gamma = 0.5 + 0.5erf\left(4\frac{T - \frac{T_{liq}+T_{sol}}{2}}{T_{liq} - T_{sol} + \epsilon}\right), \tag{1.21}$$

where $T_{liq}$, $T_{sol}$, $\epsilon$, are liquidus temperature, solidus temperature, and a small number used to avoid division by zero.

**Enthalpy Transformation Method**

In the enthalpy transformation approach, introduced by Cao et al. [26], temperature is expressed as a function of enthalpy to represent energy equation based a single variable.

$$T(H) = \Gamma(H)\, H + S(H), \tag{1.22}$$

where

$$\Gamma(H) = \begin{cases} \frac{k_s}{C_{p_s}} & H \leq 0 \\ 0 & 0 \leq H \leq L \\ \frac{k_l}{C_{p_l}} & H > L \end{cases} \tag{1.23}$$

and

$$S(H) = \begin{cases} 0 & H \leq 0 \\ 0 & 0 \leq H \leq L \\ \frac{-Lk_l}{C_{p_l}} & H > L \end{cases} \tag{1.24}$$

where $L$, $C_{p_l}$, $k_l$, $C_{p_s}$, and $k_s$, are enthalpy of fusion, heat capacity of liquid, conductivity of liquid, heat capacity of solid, and conductivity of solid, respectively. Substituting the temperature into the energy equation yields,

$$\frac{\partial \rho H}{\partial t} + \nabla \cdot (\rho \mathbf{u} H) = \nabla^2(\Gamma H) + \nabla^2(S), \tag{1.25}$$

which is based on a single variable, the enthalpy $H$. Using this method, an algorithm (Voller and Cross [23]) is needed to obtain the solid fraction from the enthalpy values in the numerical domain. This method is used by Pasandideh-Fard et al. [27] for simulation of tin droplet solidification which suggested to give reasonable results compared to experimental results. Raessi and Mostaghimi [28], also used this method for simulation of tin droplet solidification.

### 1.4.2 The Front-Tracking Method

Unverdi and Tryggvason [29] proposed a method named front tracking for tracking interfaces in multi-phase flows. Juric and Tryggvason [30] utilized this approach for solving solidification problems. In this method, the interface is marked by connected points. Marker points are used to advect the interface and consequently updating the material properties throughout the domain. In the proposed front-tracking approach heat equation is represented by a simple heat equation as follows:

$$\frac{\partial \rho C_P T}{\partial t} = \nabla \cdot (k \nabla T) + Q, \tag{1.26}$$

where $Q$ is a source term in energy equation representing the liberation of latent heat of fusion at the interface:

$$Q = \int_f q \delta(x - x_f) da, \tag{1.27}$$

where q is the heat source at the interface and $\delta$ represents the delta function which is zero all over the domain except at the interface. The idea of representing the heat of fusion by source term is similar to enthalpy method. However in front-tracking method we explicitly track the interface and its detailed micro-structure . As a result we can precisely locate the interface and express the latent heat release as a source term. One of the major concerns in front-tracking method is constructing the interface. The interface is comprised of massless points connected to each other by elements. The points at the interface can be stored without any special order. However the elements connecting the points at the front have information about their points. In order to calculate the latent heat at the interface we can use Stefan condition at the interface:

$$q = [k_s \nabla T - k_l \nabla T] \cdot \mathbf{n}, \tag{1.28}$$

where $k_s$, $k_l$, and $\mathbf{n}$ represent solid heat conductivity, liquid heat conductivity, and normal to interface, respectively. Accurate prediction of $q$ is a challenging step in numerical simulation of solidification because special care should be taken to calculate gradient of temperature in both liquid and solid regions. In order to deal with this problem Alexiades [31] proposed the following relation for heat release at the interface as a function of temperature:

$$q = \left[ L_H + (C_{Pl} - C_{Ps})(T_f - T_m)) \right] v_n. \tag{1.29}$$

where $v_n$, $T_f$, and $T_m$ represent normal velocity of the solidifying interface, interface temperature, and mean temperature, respectively. Considering the effect of Gibbs-Thomson temperature condition one can use the following relation to calculate normal

velocity of the solidifying front.

$$T_f - T_m + \frac{T_m(C_{Pl} - C_{Ps})}{L}\left(T_f \ln\frac{T_f}{T_m} + T_m - T_f\right) + \frac{\gamma(\mathbf{n})T_m}{L}\kappa + \frac{v_v}{\nu(\mathbf{n})} = 0. \tag{1.30}$$

In order to differentiate the material properties of liquid, and solid an indicator function can be used similar to enthalpy methods. However, in front-tracking approach we can accurately construct the indicator function from the known position of the interface. Using the indicator function we can update the material properties throughout the domain.

$$C(\mathbf{x}) = C_l + (C_s - C_l)I(\mathbf{x}),$$

where $C_l$, $C_s$, and $C(\mathbf{x})$ are liquid, solid, and weighted average of properties throughout the computational domain. The principal disadvantage of explicit method such as front-tracking, is the fact that spacial care is required when dealing with topological changes such as merging or breaking.

### 1.4.3 The Phase Field Method

Similar to enthalpy method, the phase field method utilizes an indicator function to identify liquid and solid phases. However, instead of using a scalar function ranging from zero to one, phase field method uses an indicator function ranging from -1 to 1. So the phase field function can be defined by:

$$\phi(\mathbf{x}, t) = \begin{cases} 1 & \text{if } \mathbf{x} \text{ is in the liquid phase} \\ -1 & \text{if } \mathbf{x} \text{ is in the solid phase} \end{cases} \tag{1.31}$$

The interface in the phase field method is defined as the region in which $-1 < \phi < 1$. The heat equation in the phase-field framework can be written as,

$$\frac{\partial \rho C_P T}{\partial t} + \frac{L}{2}\frac{\partial \phi}{\partial t} = \nabla \cdot (k \nabla T), \tag{1.32}$$

where $\frac{\partial \phi}{\partial t}$ expresses the displacement of interface location. In order to calculate the derivative of phase field with respect to time, one can use the following relation:

$$\nu \frac{\partial \phi}{\partial t} = -\frac{\delta F}{\delta \phi}, \tag{1.33}$$

where $\nu$ is a parameter that determines the thickness of the interface, and $\frac{\delta F}{\delta \phi}$ represents the variational derivative of $F$ with respect to $\phi$. In this relation, $F$ represents the free energy which is a function of $\phi$. The most important characteristic of phase field methods is sharp variation of phase field at the interface which motivates the utilization

of an adaptive grid refinement strategy. As a matter of fact, as it is shown in Merriman et al. [32] if the grid size is not proportional to $\nu$, the numerical results are not generally accurate. In contrast with front-tracking method that exact location of interface is known, the phase field method has merely an approximation of the interface location which thus implied a less accurate results near the interface. Moreover, formulating a phase field model needs an asymptotic expansion analysis be performed using the $\nu$ parameter which determines the interface thickness. As a result only in the limit as $\nu \to 0$ the phase field model converges to a sharp interface model. In this sense, even if second order numerical discretizations are utilized, the overall accuracy of the phase field method is first order accurate.

### 1.4.4 The Level-Set Method

In the level-set method (Osher and Fedkiw [33]), the interface is represented as the zero-contour of a higher dimensional function called level-set function. The level-set function is defined as the signed distance function to the interface. As a result we have negative and positive values at different regions while at the interface the level-set is identically zero.

$$\phi(\mathbf{x}) = \begin{cases} +d & \text{if } \mathbf{x} \text{ is in the liquid phase} \\ -d & \text{if } \mathbf{x} \text{ is in the solid phase} \\ 0 & \text{if } \mathbf{x} \text{ is on the interface} \end{cases} \tag{1.34}$$

where $d$ is distance to the interface. In contrast to front-tracking, phase-field and enthalpy methods, in the level-set method heat equation is represented without source term as follows:

$$\frac{\partial \rho C_P T}{\partial t} \nabla \cdot (\rho C_P \mathbf{u} T) = \nabla \cdot (k \nabla T)\,. \tag{1.35}$$

This equation is solved for the whole domain using a simple first or second order discretization. However at the interface the ghost cell method of Gibou et al. [34] can be used to consider the discontinuities and apply boundary conditions at the interface. The interface location can be evaluated using the level-set values using the following equation:

$$\mathbf{x}_\Gamma = \mathbf{x} - \phi(\mathbf{x}) \nabla \phi(\mathbf{x}). \tag{1.36}$$

Where $x_\Gamma$ is the location of interface. The interface in the level-set method evolves under the velocity field calculated from the following equation.

$$\rho L_H v_n = [k_s \nabla T - k_l \nabla T] \cdot \mathbf{n}, \tag{1.37}$$

where $v_n$ is the normal velocity of the interface. The latent heat of fusion which is one of the major challenges in simulation of solidification process, is included in the

calculation of normal velocity at the interface. As a result, level-set method can provide a sharp interface solution without explicitly tracking the interface.

The major advantage of implicit representation of a moving front is its capability in treating the complex topology changes such as pinching and merging. This is in contrast to explicit tracking the interface which needs special consideration in dealing with topology changes specially in three dimensions. On the other hand, front tracking approach, is more accurate in terms of mass conservation. Enthalpy and phase field methods also adopt an implicit formulation using volume fraction of one phase in each computational cells. These methods are conserving mass while are more complicated when it comes to accurately evaluating the interface properties such as curvature. Moreover, in these methods exact location of the interface is unknown and we are dealing with a interface region.

## 1.5 Numerical Simulation of Droplet Solidification

During the last decade many scientists endeavored to simulate droplet solidification using available methods for solving multiphase flows. However, the physics of the droplet solidification is far away from accurately modeled. The complexity of simulation of droplet solidification process is due to dealing with three phases which means we need to deal with more than one sharp interface. One of the key difficulties in simulation of droplet solidification process is tri-junction point where three phases come into contact. The angle between droplet surface and solidifying front is a fixed value which may change continuously during the solidification process. Another difficulty in numerical modeling of droplet freezing is accurately predicting the freezing front inside the droplet. Consequently we need to deal with discontinuities and jump conditions inside the droplet. Furthermore, density expansion during phase change should be taken into account in numerical models. Based on available experimental results in the literature (Marin et al. [12], Jin et al. [13]) we know that liquid expansion or shrinkage during freezing process crucially affects the final morphology of the solidified droplet. For example, many researchers suggested that the droplet expansion during freezing process is a main cause of protrusion formation on top of the droplet after complete solidification.

Pasandideh-Fard et al. [27] simulated droplet impact including heat transfer and solidification. They intended to simulate impact molten tin droplets onto stainless steel surfaces. They extended the three-dimensional model presented by Bussmann et al. [35] to take into account the heat transfer. Pasandideh-Fard et al. [27] utilized enthalpy transformation method to consider release of latent heat of fusion. However, since enthalpy method generally is not able to handle discontinuities, their model can only be

justified for modeling alloys because of existence of the mushy zone at the solidifying interface. However, utilization of the model presented by Pasandideh-Fard et al. [27] is not justifiable for water or pure material solidification because of discontinuities at the interface. In order to set the velocity to zero Pasandideh-Fard [36] used a variant of fixed velocity approach originally presented by Voller [20]. In this approach in order to have zero velocities at the solidified region they used an indicator function representing water volume fraction.

Raessi and Mostaghimi [28] presented a model which is an extension of the work of Pasandideh-Fard et al. [27] to simulate metal droplet freezing taking into account the density change. They applied the model to investigate the effect of density variation during solidification of an impacting molten tin droplet on a substrate. The model presented by Raessi and Mostaghimi [28] is a two-phase model which neglects the effect of tri-junction point which is of the utmost importance in droplet freezing process. They used a simplified model by only taking into account the liquid and solid phases while the actual droplet physics is a three-phase phenomenon.

Vu et al. [2] extended the front tracking method of Al-Rawahi and Tryggvason [37] to simulate two dimensional three-phase droplet freezing process. They used front-tracking to capture liquid-air and liquid-solid interfaces. They applied a constant angle at the tri-junction point between solidifying and droplet interfaces. In addition, they considered water expansion as a result of phase change to study the variation of droplet interface. In spite of the accurate prediction of droplet morphology they overestimated the freezing time because in their model effect of volume expansion in heat transfer is neglected.

As reviewed in this section, there is a variety of models presented in the literature for modeling two phase solidification process. Among the models, it has been known that the front-tracking and level-set methods are able to handle many physical occurrences during the freezing process especially for pure materials where there is a discontinuity at the interface. During the last decade many scholars endeavored to extend the two phase solidification to three-phase solidification to simulate freezing of impacting droplets on solid substrates. Enthalpy and front-tracking methods have been already improved to simulate droplet solidification. However, those methods are not inherently capable of handling complicated physical mechanisms in solidification process. For instance, enthalpy method is developed based on the assumption that there is a mushy zone at the solidifying front which not physical for pure materials. As a result, the models developed using enthalpy method are only justified for simulation of solidification of alloys. On the other hand, in spite of the fact that front-tracking has been effectually used for modeling freezing process of pure materials in several papers, the model requires special care in the case of complicated morphological changes such as pinching and merging.

The level-set method has been demonstrated to be a powerful approach for treating multiphase flows. Since the location of the interface is tracked implicitly, complex morphological changes can be treated accurately. In addition, the method has been improved during the last decade to apply jump conditions and discontinuities at the front. As a result level-set method is an appropriate approach for simulation of a variety of multiphase flows including solidification of pure materials. However, level set method is merely developed for modeling two-phase solidification and there is a gap in the literature to extend the level-set method for three-phase solidification process. It is therefore the objective of this study to develop a numerical model based on the level-set method to simulate droplet solidification that takes into account several physical phenomenon.

## 1.6 Objectives and Thesis Outline

The aim of current study is to propose a numerical model based on the level-set method for modelling water droplet freezing on cold plates. We developed a multiple level-set method for capturing two moving interfaces: liquid-gas; liquid-solid. In general objectives of the current study can be summarized as follows:

- Extend level-set method to solve three-phase problems
- Impose fixed temperature at the moving solidifying front
- Impose a fixed angle at the tri-junction point
- Modify heat equation to consider effect of density expansion on the rate of solidification
- Modify mass conservation equations in order to take into account the effect of density expansion

The structure of this thesis is based on the stages undertaken in developing the model. In Chapter 2, we described level-set method and the computational algorithm incorporated to simulate two-phase solidification process. Moreover, detailed numerical implementation of continuity and Navier-Stokes equations followed by modifications required for considering volume expansion during the phase change is presented. In Chapter 3, we use standard benchmark problems to validate the accuracy of proposed numerical approach. Then the numerical model will be utilized to investigate physics of water droplet solidification. Chapter 5, the last chapter, summarizes the thesis and provides conclusions and future works.

# Chapter 2

# Computational Methodology

In this chapter the details of numerical methods used for simulation of water droplet solidification will be presented. In order to model physics of water droplet freezing process we need to solve and couple multiple physics (Fig. 2.1). We start the chapter by describing numerical details of level-set method and heat equation in the presence of thermal jumps at the solidifying interface. The methods utilized to solve Navier-Stokes equations for two-phase flows will be described afterwards. We will present the proposed model and modifications required for extending level-set method for three-phase problems. Moreover, the details of coupling heat transfer and fluid dynamic equations to take into account the density expansion will be discussed in the last section.

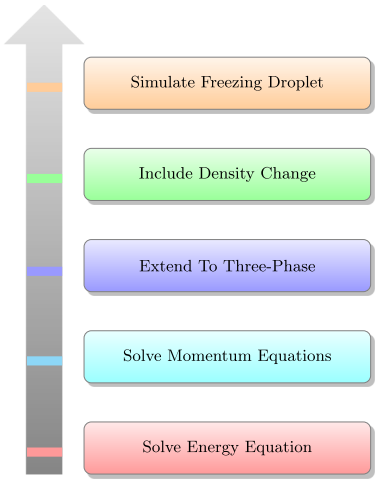


Figure 2.1: Schematic of procedure of numerical modelling of water droplet freezing process

## 2.1 Level-Set Method

Interface tracking is one of the fundamental parts of numerical simulation of multiphase flows. One of the most efficient and accurate methods proposed by Osher and Fedkiw [33] is level-set method which is level-sets of a higher dimensional function (Fig. 2.2). The level-set method is capable of naturally handling complicated topological changes such as pinching and merging. In this chapter we introduce the level set method and its application in simulation of solidification physics.

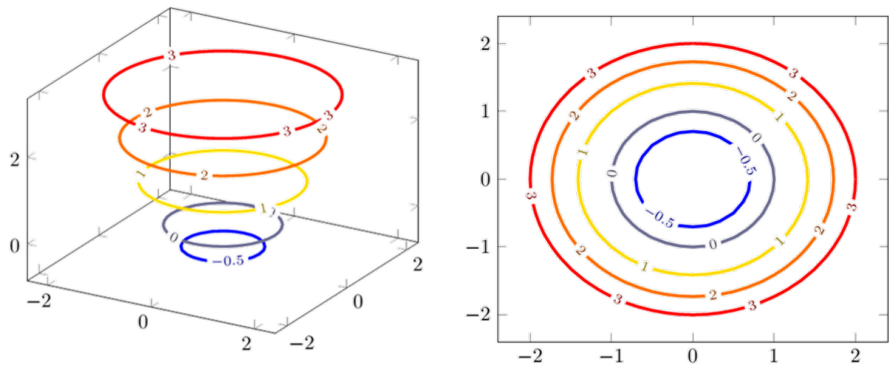

Figure 2.2: Level-set representation of an interface in two spatial dimensions

An interface, $\Gamma$, in level-set method is represented as the zero-contour of a higher dimensional function which is defined as signed distance function to the interface.

$$\phi(\mathbf{x}) = \begin{cases} +d & \text{if } \mathbf{x} \text{ is in the liquid phase} \\ -d & \text{if } \mathbf{x} \text{ is in the solid phase} \\ 0 & \text{if } \mathbf{x} \text{ is on the interface} \end{cases} \tag{2.1}$$

where $d$ is the distance to interface and defined as;

$$d(\mathbf{x}, t) = \min(\mathbf{x} - \mathbf{x}_I(t)) \tag{2.2}$$

where $\mathbf{x}_I$ denotes the position of the interface. Signed distance functions posses a number of properties that are useful in numerical treatments of interfaces. One of the most important characteristic of signed distance functions is,

$$|\nabla \phi| = 1 \tag{2.3}$$

In practice, however by moving the level-sets this condition may be violated. In order to avoid numerical difficulties associated with the signed distance property of level-sets we perform a re-initialization step by which we ensure that the value of the gradient of the level-set function is equal to 1. Sussman et al. [38] proposed the reinitialization

equation:

$$\frac{\partial \phi}{\partial \tau} + S_e(\phi^0)\left(|\nabla \phi| - 1\right) = 0, \tag{2.4}$$

to convert a level-set function to a signed distance function. In this equation the $S_e$ represents a smoothed-out sign function, $\phi^0$ is initial level-set, and $\tau$ is a fictitious time controlling the width of the region around the zero level-set in which the level-sets are signed distanced. A signed distance level-set function can be used to project any point onto the interface using the following equation.

$$\mathbf{x}_\Gamma = \mathbf{x} - \phi(\mathbf{x})\nabla\phi(\mathbf{x}) \tag{2.5}$$

Another characteristic of a signed distance function is having a kink at the interface where $d = 0$. Because of this characteristic we should be cautious in calculation of gradient near the interface which are explained in Section. 2.2.3. Moreover, signed distance functions are monotonic across the interface and can be differentiated accurately.

In each time step we need to advect the level-set function with an appropriate velocity field. The evolution of the interface will be performed implicitly by solving the following equation,

$$\frac{\partial \phi}{\partial t} + \mathbf{u} \cdot \nabla \phi = 0 \tag{2.6}$$

The level-set advection equation can also be written in the form of normal velocity to the interface.

$$\frac{\partial \phi}{\partial t} + v_n |\nabla \phi| = 0 \tag{2.7}$$

where $v_n = \mathbf{u} \cdot \mathbf{n}$. Solving the advection equation can be complicated if the velocity is only defined at the interface. This condition happens in the case of solidification process where velocity of the solidifying front is only defined at the interface. In this situations we need to extend the velocity off the interface to have velocity in all grid cells in the domain. The details of velocity extension will be explained later in Section. 2.2.4.

Accuracy of numerical results using level-set method depends on the numerical schemes used for spatial and temporal discretizations. In the following sections we represent the details of numerical schemes used to solve differential equations utilized in level-set method.

### 2.1.1 Hamilton-Jacobi ENO

In order to improve spatial discretizations we may use higher order and more accurate approximations for single sided gradients. Hamilton-Jacobi ENO proposed by Shu and Osher [39] can be used to improve numerical discretizations. In this thesis we use second order accurate ENO scheme.

Assume we want to evaluate one sided gradients of the variable $\phi$. We start with the zeroth divided differences of $\phi$ defined at cell centers as:

$$D_i^0\phi = \phi_i, \tag{2.8}$$

while the first divided difference of $\phi$ are defined at the faces between grid cells as

$$D_{i+1/2}^1\phi = \frac{D_{i+1}^0\phi - D_i^0\phi}{\Delta x} \tag{2.9}$$

$$D_{i-1/2}^1\phi = \frac{D_i^0\phi - D_{i-1}^0\phi}{\Delta x}, \tag{2.10}$$

Note that the first divided differences are simply first order backward and forward approximations of the derivatives. In order to obtain second order approximations we define the second divided differences at cell centers as follows:

$$D_i^2\phi = \frac{D_{i+1/2}^1\phi - D_{i-1/2}^1\phi}{2\Delta x} \tag{2.11}$$

The divided differences can be used to form a polynomial of the form

$$\phi(x) = Q_0(x) + Q_1(x) + Q_2(x) \tag{2.12}$$

which can be differentiated as

$$\phi_x(x_i) = Q_1'(x_i) + Q_2'(x_i) \tag{2.13}$$

To evaluate first order gradients we use

$$Q_1'(x_i) = D_{k+\frac{1}{2}}^1\phi, \tag{2.14}$$

where $k$ should be substituted by $i-1$ to calculate $\phi^-(x)$, and $i$ for $\phi^+(x)$. For higher order accuracy we need to obtain a relation for $Q_2'$. Since it is desirable to avoid discontinuities for evaluation of gradients we use the following second order approximation.

$$Q_2'(x_i) = c(2(i-k)-1)\Delta x \tag{2.15}$$

where $c = D_k^2\phi$ if $|D_k^2| < |D_{k+1}^2\phi|$, otherwise $c = D_{k+1}^2\phi$.

### 2.1.2 Advection Equation

An interface can be evolved under a velocity field which is normal to the interface and is dependent on the characteristic of the interface itself similar to evolution of

solidifying front. In this condition the velocity is normal to the interface and equation of motion can be represented as,

$$\frac{\partial \phi}{\partial t} + v_n |\nabla \phi| = 0, \tag{2.16}$$

where $v_n$ is the normal velocity and can be positive or negative. In the case of spatially constant interface it can be shown that if the level-set function is initially signed distance, it will remain signed distance over time.

The advection equation of level-set is a Hamilton-Jacobi type equation which has a general form of

$$\frac{\partial \phi}{\partial t} + H(\nabla \phi) = 0 \tag{2.17}$$

where H is a function of first derivate of level-set function which depends on time and space.

The Hamiltonian function can be spatially discretized using Godunov's method,

$$H^n(\nabla \phi)_{ij} = \begin{cases} \sqrt{\max((a^+)^2,(b^-)^2) + \max((c^+)^2,(d^-)^2)}, & \text{if } v_n < 0 \\ \sqrt{\max((a^-)^2,(b^+)^2) + \max((c^-)^2,(d^+)^2)}, & \text{if } v_n > 0 \end{cases} \tag{2.18}$$

where

$$\begin{aligned} a &= D_x^- \phi_{i,j} = \frac{\phi_{i,j} - \phi_{i-1,j}}{\Delta x} \\ b &= D_x^+ \phi_{i,j} = \frac{\phi_{i+1,j} - \phi_{i,j}}{\Delta x} \\ c &= D_y^- \phi_{i,j} = \frac{\phi_{i,j} - \phi_{i,j-1}}{\Delta x} \\ d &= D_y^- \phi_{i,j} = \frac{\phi_{i,j+1} - \phi_{i,j}}{\Delta x} \end{aligned}$$

which is a first order, consistent, monotone scheme. In these equations the $a^+$ or $a^-$ represents positive part or negative part of $a$ which are defined as $\max(a,0)$ and $\min(a,0)$, respectively. In order to achieve higher order accuracy in discretization we can use second order Hamilton-Jacobi ENO one sided approximations represented in Section 2.1.1

For temporal discretization we use third order Total Variation Diminishing Runge-Kutta scheme. Third order Runge Kutta is a combination of multiple Euler steps (Shu and Osher [39]). We take the first step to calculate a temporary $\phi^{n+1}$ at time $t^{n+1}$;

$$\frac{\phi^{n+1} - \phi^n}{\Delta t} + H_G(\phi^n) = 0, \tag{2.19}$$

followed by another step to find temporary $\phi^{n+2}$,

$$\frac{\phi^{n+2} - \phi^{n+1}}{\Delta t} + H_G(\phi^{n+1}) = 0. \tag{2.20}$$

The $\phi^{n+1/2}$ can be evaluated by averaging of $\phi^n$ and $\phi^{n+2}$ as,

$$\phi^{n+1/2} = \frac{3}{4}\phi^n + \frac{1}{4}\phi^{n+2}, \tag{2.21}$$

followed by another Euler step to calculate $\phi^{n+3/2}$ as,

$$\frac{\phi^{n+3/2} - \phi^{n+1/2}}{\Delta t} + H_G(\phi^{n+1/2}) = 0. \tag{2.22}$$

which is finally used to update $\phi^{n+1}$ by averaging as follows,

$$\phi^{n+1} = \frac{1}{3}\phi^n + \frac{2}{3}\phi^{n+3/2}. \tag{2.23}$$

that produces a third-order accurate approximation of $\phi$.

In many cases we need to evolve level-sets under externally generated velocity fields. The equation of level-set advection is defined by

$$\frac{\partial \phi}{\partial t} + \mathbf{u} \cdot \nabla \phi = 0. \tag{2.24}$$

Once $\mathbf{u}$ and $\phi$ are defined at grid cell centers we can use upwind advection scheme to evolve level-sets in time. In upwinding scheme we use one sided forward or backward approximations of the gradients based on the sign of velocity. If $u_i > 0$ it means that the $\phi_{i,j}$ will move from left to right which implies that backward approximation of gradients should be used. The same thing applies in the vertical direction. On the other hand if $u_i < 0$, the values of $\phi$ will move from right to left which implies that we should use forward approximations for calculation of gradients. The combination of first order Euler time discretization and the upwind difference scheme is consistent and Stability can be enforced by using Courant-Friedreichs-Lewy (CFL) condition. The CFL condition asserts that the numerical wave should propagate at least as the physical waves which leads to the CFL time step restriction of

$$\Delta t < \frac{\Delta x}{\max|u|}, \tag{2.25}$$

where $\Delta x$ is grid size, and $\max|u|$ is the largest absolute value of velocity over the entire computational domain.

### 2.1.3 Reinitialization

As stated before a lot of simplifications can be made if level-sets are signed distance function from the interface. However, as the level-sets evolves, it may drift away from its initialized signed distance function. As a result, depending on the sensitivity of our implementations we need to reinitialize level-sets to ensure that level-sets are signed distance function. Sussman et al. [38] provided the following equation for reinitialization of level-sets.

$$\frac{\partial \phi}{\partial t} + S(\phi_0)\left(|\nabla \phi| - 1\right) = 0 \tag{2.26}$$

where $S(\phi_0)$ is a sign of level-set. Solving this equation using fictitious time to reach steady state condition will create a signed distant level-set field.

In discretization of Equation. 2.26 we use Godunov's method similar to the advection of level-set with internally generated velocity field as follows,

$$\phi_{i,j}^{n+1} = \phi_{i,j}^{n} - \Delta t S_e(\phi_{i,j}^{0}) H(\phi_{i,j}^{n}), \tag{2.27}$$

where $S_e(\phi_{i,j}^{0})$ is smeared out sign function of initial level-set function. It is shown we can obtain better results using the following smeared out sign function,

$$S_e(\phi_{i,j}) = \frac{\phi_{i,j}}{\sqrt{\phi_{i,j}^2 + \epsilon^2}} \tag{2.28}$$

where the grid size $\Delta x$ can be used instead of $\epsilon$. $H(\phi_{i,j}^{0})$ is Hamiltonian function which can be discretized as,

$$H^n(\phi)_{ij} = \begin{cases} \sqrt{\max((a^+)^2,(b^-)^2) + \max((c^+)^2,(d^-)^2)} - 1, & \text{if } \phi_{i,j}^{0} > 0 \\ \sqrt{\max((a^-)^2,(b^+)^2) + \max((c^-)^2,(d^+)^2)} - 1, & \text{if } \phi_{i,j}^{0} < 0 \end{cases} \tag{2.29}$$

We can increase the accuracy of our approximations by using second order Hamilton-Jacobi ENO scheme.

Min [40] discussed the difficulties associated with the reinitialization of level-set process using the above method. They represented that using the artificially smeared-out sign function the interface moves and would decrease the volume inside the interface considerably. In order to avoid artificial movement of interface over time, we use the subcell modifications presented by Min [40]. Near the interface, finite difference approximations of one sided derivations we impose the condition that $\phi = 0$ whenever $\phi^0 = 0$. For brevity we consider modifications made for $D^+\phi_{i,j}$ in the case of $\phi_{i,j}\phi_{i+1,j} < 0$ which means that interface is located between $\phi_{i,j}$ and $\phi_{i+1,j}$. In this

situation the distance to the interface can be obtained by

$$\Delta x^{+} = \Delta x \frac{\phi^{0}_{i,j}}{\phi^{0}_{i,j} - \phi^{0}_{i+1,j}} \tag{2.30}$$

Now by imposing $\phi = 0$ on the calculated interface point $(x_\Gamma, y_\Gamma)$, the forward one sided derivative can be modified as,

$$D^{+}_{x}\phi_{i,j} = \frac{0 - \phi_{i,j}}{\Delta x^{+}} - \frac{\Delta x^{+}}{2} minmod(D_{xx}\phi_{i,j}, D_{xx}\phi_{i+1,j}) \tag{2.31}$$

where $minmod(x,y)$ is defined as,

$$minmod(x,y) = \begin{cases} x & \text{if } |x| > |y| \\ y & \text{otherwise} \end{cases} \tag{2.32}$$

For the backward derivative we first calculate $\Delta x^{-}$ as,

$$\Delta x^{-} = \Delta x \frac{\phi^{0}_{i,j}}{\phi^{0}_{i,j} - \phi^{0}_{i-1,j}} \tag{2.33}$$

then we can calculate backward derivations as,

$$D^{-}_{x}\phi_{i,j} = \frac{\phi_{i,j} - 0}{\Delta x^{-}} + \frac{\Delta x^{-}}{2} minmod(D_{xx}\phi_{i,j}, D_{xx}\phi_{i-1,j}) \tag{2.34}$$

The discretization presented here can be extended to other directions in a direction by direction fashion. The discretization is second order accurate with subcell resolution near the interface.

### 2.1.4 Poisson Helmholtz Equation

Generally Poisson-Helmholtz equation is the major building block for solving differential equation encountered in fluid flow and heat transfer. The simulation of many diffusion-dominated phenomena require the solution of Poisson Helmholtz type equation. The general form of the equation can be written as follows

$$\nabla \cdot (\beta \nabla a) + \lambda a = b, \tag{2.35}$$

where $\beta$ and $\lambda$ are coefficients that can be spatially constant or variable. Linearity is an important aspect of the resulting system. This characteristic can be used to estimate the solution by successive corrections to an initial guess. Assume that $\hat{a}_{i,j}$ is an approximation of the exact solution $a_{i,j}$, and $da$ is the difference between exact and

approximate solution defined as,

$$da = a - \hat{a} \tag{2.36}$$

If we define Poisson operator, $\mathcal{L}(a)$ as,

$$\mathcal{L}(a) = \nabla \cdot (\beta \nabla a) + \lambda a, \tag{2.37}$$

the correction of the approximate solution can be obtained from,

$$\mathcal{L}(da) = \mathcal{L}(a) - \mathcal{L}(\hat{a}) = b - \mathcal{L}(\hat{a}) \tag{2.38}$$

where $\mathcal{L}(da)$ is the error or residual of the solution. In each iteration we need to calculate discretized residuals and using a relaxation operation we can calculate the correction to approximate calculations. The iteration can be continued until the residual is less than a predefined criteria. The Poisson-Helmholtz equation can be discretized with second-order accuracy as,

$$\frac{\beta_{i+\frac{1}{2}} \left( \frac{a_{i+1} - a_i}{\Delta x} \right) - \beta_{i-\frac{1}{2}} \left( \frac{a_i - a_{i-1}}{\Delta x} \right)}{\Delta x} + \lambda_i a_i = b_i \tag{2.39}$$

where $\beta$ is defined at cell faces and other variables are defined at cell centers. Hence the residual can be calculated as,

$$\mathcal{R}(\hat{a}_i) = b_i - \frac{\beta_{i+\frac{1}{2}} \left( \frac{\hat{a}_{i+1} - \hat{a}_i}{\Delta x} \right) - \beta_{i-\frac{1}{2}} \left( \frac{\hat{a}_i - \hat{a}_{i-1}}{\Delta x} \right)}{\Delta x} - \lambda_i \hat{a}_i \tag{2.40}$$

Corrections are calculated from the following discretized relaxation operation.

$$da_i = \frac{\Delta x^2 (\mathcal{R}(\hat{a}_i) - \lambda_i da_i) - \beta_{i+\frac{1}{2}} \hat{a}_{i+1} + \beta_{i-\frac{1}{2}} \hat{a}_{i-1}}{\beta_{i+\frac{1}{2}} - \beta_{i-\frac{1}{2}}} \tag{2.41}$$

In each iteration we add the corrections calculated in this step to the approximate solution of previous iteration. The procedure continues until the residual is less than the specific criteria.

## 2.2 Poisson Equation on Axisymmetric Domains

In this section we describe the modifications required for solving Poisson equation in axisymmetric domains. The Poisson equation on axisymmetric grids can be written as,

$$\frac{1}{r} \frac{\partial}{\partial r} \left( r \beta \frac{\partial a}{\partial r} \right) + \frac{\partial}{\partial y} \left( \beta \frac{\partial a}{\partial y} \right) = b \tag{2.42}$$

If we multiply both sides of the equation by $r$ we obtain,

$$\frac{\partial}{\partial r}\left(r\beta\frac{\partial a}{\partial r}\right)+\frac{\partial}{\partial y}\left(r\beta\frac{\partial a}{\partial y}\right)=rb \tag{2.43}$$

by defining $\hat{\beta}=r\beta$, and $\hat{b}=rb$, we can wirte,

$$\frac{\partial}{\partial r}\left(\hat{\beta}\frac{\partial a}{\partial r}\right)+\frac{\partial}{\partial y}\left(\hat{\beta}\frac{\partial a}{\partial y}\right)=\hat{b}. \tag{2.44}$$

which is similar to Poisson equation in Cartesian grids and can be discretized using the same approach described previously.

### 2.2.1 Poisson Helmholtz Equation on Irregular Domains

In the case regular Cartesian grids we can use the discretization presented in the previous section to solve Poisson equation. However, there are many cases that we want to solve Poisson equations on irregular domains that are represented by level-set. The domain is divided into two different regions by the zero-th level set. If we want to impose Dirichlet boundary condition, we need to use special discretization for the Poisson equation.

First, assume that the interface $x_I$ is located between $x_i$ and $x_{i+1}$ and we want to apply Dirichlet boundary condition ($u=u_I$) at the interface. The second order discretization of Poisson equation for grid cells situated at the left of the interface is the same as Eq. 2.126. However, the value of $x_{i+1}$ is not valid for discretizing at $x_i$. At this point we use ghost cell method to impose Dirichlet boundary condition at the interface.

$$\frac{\beta_{i+\frac{1}{2}}\left(\frac{a^G_{i+1}-a_i}{\Delta x}\right)-\beta_{i-\frac{1}{2}}\left(\frac{a_i-a_{i-1}}{\Delta x}\right)}{\Delta x}+\lambda_i a_i=b_i \tag{2.45}$$

where $a^G_{i+1}$ is the ghost value at the right of the interface. We approximate $a^G_{i+1}$ using linear extrapolation as,

$$a^G_{i+1}=\frac{a_I+(\theta-1)a_i}{\theta} \tag{2.46}$$

where $\theta$ is defined as $\theta=\frac{|\phi|}{\Delta x}$. In the case of $\theta<1$ we use $a_i$ instead of $a_I$ to avoid poor behavior of the extrapolations. Now by substituting Eq. 2.46 into Eq. 2.45 yields,

$$\frac{\beta_{i+\frac{1}{2}}\left(\frac{a_I-a_i}{\theta\Delta x}\right)-\beta_{i-\frac{1}{2}}\left(\frac{a_i-a_{i-1}}{\Delta x}\right)}{\Delta x}+\lambda_i a_i=b_i \tag{2.47}$$

which is second order accurate. If we use the same approach for extrapolation of ghost values when interface is located between $x_i$ and $x_{i-1}$ the discretized Poisson Helmholtz

equation can be written as,

$$\frac{\beta_{i+\frac{1}{2}}\left(\frac{a_{i+1}-a_i}{\Delta x}\right)-\beta_{i-\frac{1}{2}}\left(\frac{a_i-a_I}{\theta\Delta x}\right)}{\Delta x}+\lambda_i a_i=b_i \tag{2.48}$$

In situations where $\beta$ is defined at grid cell centers, the face centered values, $\beta_{i+\frac{1}{2}}$ can be obtained from the ghost values using the following equation.

$$\beta_{i+\frac{1}{2}}=\frac{\beta_i+\beta^G_{i+1}}{2}, \tag{2.49}$$

noting that the ghost value is calculated as,

$$\beta^G_{i+1}=\frac{\beta_I+(\theta-1)\beta_i}{\theta} \tag{2.50}$$

For higher dimensions we use the above mentioned approach in a dimension by dimension manner.

### 2.2.2 Energy Equation

General form of energy equation can be written in the following form.

$$\rho\frac{\partial E}{\partial t}+\rho\mathbf{u}\cdot\nabla E=\nabla\cdot(k\nabla T) \tag{2.51}$$

where $k$, $T$ represent the thermal conductivity and temperature, respectively. The energy equation can be written based on the temperature as follows,

$$\rho C_p\frac{\partial T}{\partial t}+\rho C_p\mathbf{u}\cdot\nabla T=\nabla\cdot(\kappa\nabla T) \tag{2.52}$$

which can be simplified to the following form if the advection term is negligible.

$$\rho C_p\frac{\partial T}{\partial t}=\nabla\cdot(\kappa\nabla T) \tag{2.53}$$

Implicit Euler temporal discretization of the equation leads to the following equation.

$$\frac{T^{n+1}-T^n}{\Delta t}=\nabla\cdot\left(\hat{\kappa}\nabla T^{n+1}\right) \tag{2.54}$$

which is first order accurate in time and second order accurate in space. Hence in order to have second order accuracy we need to choose $\Delta t$ proportional to $\Delta x^2$. The Crank-Nicolson scheme can be used instead to achieve second order accuracy in time and space. Temporal discretization of using Crank-Nicolson can be written as,

$$\frac{T^{n+1}-T^n}{\Delta t}=\frac{1}{2}\nabla\cdot\left(\hat{\kappa}\nabla T^{n+1}\right)+\frac{1}{2}\nabla\cdot\left(\hat{\kappa}\nabla T^n\right) \tag{2.55}$$

which can be written in the form of Poisson-Helmholtz equation as,

$$\nabla\cdot\left(\hat{\kappa}\nabla T^{n+1}\right)-\frac{2T^{n+1}}{\Delta t}=-\frac{2T^n}{\Delta t}-\nabla\cdot\left(\hat{\kappa}\nabla T^n\right) \tag{2.56}$$

which can be solved using the algorithm mentioned before in Section. 2.2.1.

### 2.2.3 Interface Velocity

In solidification we are dealing with Stefan type problems in which the liquid is being converted to solid at the interface. Hence the interface between liquid and solid will move with a specific velocity. The normal interface velocity can be computed using the Stefan jump condition as,

$$\rho_l L_H v_n=\kappa_l(\nabla T\cdot\mathbf{n})_l-\kappa_s(\nabla T\cdot\mathbf{n})_s \tag{2.57}$$

where $\rho_l$, $L_H$, $\kappa_l$, and $\kappa_s$ represent liquid density, latent heat of fusion, liquid heat conductivity, and solid heat conductivity, respectively. One of the challenges in level-set method is to accurately predict gradients at the interface. In order to calculate the gradients near the interface we use the approach presented by Gibou et al. [41]. Lets first consider evaluation of gradients in the liquid phase. Generally four case may happen at the interface depending on the position of the interface with respect to the cell center. Here we consider one dimension while it can be extended for higher dimensions.

**Case I** The interface is located between $x_i$, and $x_{i-1}$ and $\theta>1$. We use $T_i$ and $T_I$ to calculate gradient as,

$$\frac{\partial T}{\partial x}=\frac{T_i-T_I}{\theta\Delta x} \tag{2.58}$$

**Case II** The interface is location between $x_i$, and $x_{i-1}$ and $\theta<\Delta x$. We use $T_{i+1}$ and $T_I$ to calculate gradient as,

$$\frac{\partial T}{\partial x}=\frac{T_{i+1}-T_I}{\theta\Delta x} \tag{2.59}$$

**Case III** The interface is location between $x_i$, and $x_{i+1}$ and $\theta>\Delta x$. We use $T_i$ and $T_I$ to calculate gradient as,

$$\frac{\partial T}{\partial x}=\frac{T_I-T_i}{\theta\Delta x} \tag{2.60}$$

**Case IV** The interface is location between $x_i$, and $x_{i+1}$ and $\theta < \Delta x$. We use $T_{i-1}$ and $T_I$ to calculate gradient as,

$$\frac{\partial T}{\partial x} = \frac{T_I - T_{i-1}}{\theta \Delta x} \tag{2.61}$$

The same procedure is used for calculation of gradients in the solid phase. For higher dimensions we repeat the procedure in a dimension by dimension manner. For example for Case I the gradient can be written as,

$$\frac{\partial T}{\partial y} = \frac{T_I - T_{i,j}}{\theta \Delta y} \tag{2.62}$$

### 2.2.4 Extension Velocity

In many moving interface problems, such as Stefan type problems, the speed of the interface has significance only at the interface itself. However, having velocity discontinuity at the interface is not desirable for numerical algorithms. Moreover, in order to advect level-sets we need to have velocity of the interface defined not only at the interface but also at all grid cells around the interface. To this end, the velocity should be extrapolated from the interface to neighboring grid cells which is referred to as velocity extension.

The normal velocity in Eq. 2.7 is physically meaningful when $\phi = 0$. However, in order to solve the Eq.2.7 we need to extrapolate the normal velocity such that,

$$\lim_{x \to a} v_{ext}(x) = v_n(a) \tag{2.63}$$

where $a$ is a point on the interface ($\phi = 0$). There is a number of algorithms to construct extension velocities. One approach is to solve equation

$$\nabla v_n \cdot \nabla \phi = 0 \tag{2.64}$$

by a process called Fast Marching Method proposed by Adalsteinsson and Sethian [42]. In this approach, extension will be constructed by sweeping in the upwind direction from the interface. An alternative approach, which is utilized in this study, is to solve the following advection equation

$$\frac{\partial v_n}{\partial \tau} + S(\phi) \nabla v_n \cdot \mathbf{n} = 0 \tag{2.65}$$

where $\tau$ is a fictitious time and is not related to the domain time and $S(\phi)$ represents sign function. By solving this equation to reach steady state condition we will extrapolate normal interface velocity off the interface which are constant along lines normal to the interface. While we can use central differencing scheme for discretization of $\nabla v_n \cdot \mathbf{n}$,

one sided upwind differencing scheme is advantageous. In order to decide whether backward or forward differencing we consider $\phi_{i+1}$ and $\phi_{i-1}$. If either of these values are smaller than $\phi_i$ we use the minimum of these values to evaluate $\frac{\partial \phi}{\partial x}$. On the other hand, if both of these values are greater that $\phi_i$, we will set $\frac{\partial \phi}{\partial x} = 0$.

## 2.3 Incompressible Flows

In this section we present numerical methods for solving equations governing multi-phase flows. Firstly, we present numerical methods used for solving Navier-Stokes equations for single phase fluid flows. Afterwards, we represent numerical details of two-phase flows with discontinuities at the interface including surface tension forces.

Governing equations for fluid flow are obtained based on the two basic physical laws namely conservation of mass and momentum. The principle of conservation of mass represents that mass cannot be created nor destroyed which can be represented mathematically in the integral form as,

$$\frac{d}{dt}\int_V \rho \, dv = -\int_S \rho \mathbf{u} \cdot \mathbf{n} \, ds \tag{2.66}$$

which can be written in the form of partial differential equation as,

$$\frac{\partial \rho}{\partial t} + \nabla \cdot (\rho \mathbf{u}) = 0. \tag{2.67}$$

Since for incompressible flows the density is constant over time the conservation of mass equation simplified as,

$$\nabla \cdot \mathbf{u} = 0. \tag{2.68}$$

The equation of motion is derived by employing the conservation of momentum. The conservation of momentum states that the rate of change of fluid momentum in a fixed volume is the difference of flux across the boundaries and can be expressed in the integral form as,

$$\frac{d}{dt}\int_V \mathbf{u} \, dv = -\oint_S \rho \mathbf{u} (\mathbf{u} \cdot \mathbf{n}) \, ds + \int_V \mathbf{F}_b \, dv + \oint_S \mathbf{n} \cdot \mathbf{T} \, ds, \tag{2.69}$$

which can be written in the form of partial differential equations as,

$$\frac{\partial \rho \mathbf{u}}{\partial t} = -\nabla \cdot (\rho \mathbf{u}\mathbf{u}) + \mathbf{F}_b + \nabla \cdot \mathbf{T}. \tag{2.70}$$

where $\mathbf{F_b}$ is body force and $\mathbf{T}$ is stress tensor. The simplified form of the momentum equation for incompressible flows can be written as follows,

$$\rho\frac{\partial \mathbf{u}}{\partial t} + \rho\mathbf{u}\cdot\nabla\mathbf{u} = -\nabla p + \nabla\cdot(2\mu\mathbf{D}) + \mathbf{F}_b. \tag{2.71}$$

with $\mathbf{u} = (u,v,w)$ , the fluid velocity, $\rho = \rho(\mathbf{x},t)$ the fluid density, and $\mu = \mu(\mathbf{x},t)$ the dynamic viscosity of the fluid and $\mathbf{D}$ the deformation tensor defined as $D_{ij} = (\partial_i u_j + \partial_j u_i)/2$

### 2.3.1 Temporal Discretization

For incompressible flows the pressure should give a divergence-free velocity field at the end of each time step. The staggered in time discretization of pressure leads to the following second-order accurate discretization.

$$\rho_f\left[\frac{\mathbf{u^{n+1}} - \mathbf{u^n}}{\Delta t} + \mathbf{u}^{n+\frac{1}{2}}\cdot\nabla\mathbf{u}^{n+\frac{1}{2}}\right] = -\nabla p^{n+\frac{1}{2}} + \nabla\cdot\left[\mu_f(\mathbf{D}^n + \mathbf{D}^{n+1})\right] + \mathbf{F}_f^{n+\frac{1}{2}} \tag{2.72}$$

$$\nabla\cdot\mathbf{u}^n = 0 \tag{2.73}$$

In order to assure that the velocity field is divergence free we use the classical time splitting projection method of Chorin [43]. In this method a temporary velocity field is first found by ignoring pressure gradients using the following relation.

$$\rho_f\left[\frac{\mathbf{u}^\star - \mathbf{u^n}}{\Delta t} + \mathbf{u}^{n+\frac{1}{2}}\cdot\nabla\mathbf{u}^{n+\frac{1}{2}}\right] = \nabla\cdot\left[\mu_f(\mathbf{D}^n + \mathbf{D}^*)\right] + \mathbf{F}_f^{n+\frac{1}{2}} \tag{2.74}$$

which can be rearranged as,

$$\rho_f\frac{\mathbf{u}^\star}{\Delta t} - \nabla\cdot\left[\mu_f\mathbf{D}^\star\right] = \nabla\cdot\left[\mu_f\mathbf{D}^n\right] + \rho_f\left[\frac{\mathbf{u}^n}{\Delta t} - \mathbf{u}^{n+\frac{1}{2}}\cdot\nabla\mathbf{u}^{n+\frac{1}{2}}\right] + \mathbf{F}_f^{n+\frac{1}{2}} \tag{2.75}$$

where $\rho_f$ and $\mu_f$ are face centered density and viscosities. In this equation the right hand side only depends on the values at time $n$ and $n+\frac{1}{2}$. The resulting equation is a Poisson-Helmholtz type equation and can be solved using iterative methods. The velocity field obtained from this equation is not divergence free and should be modified in the next step by adding an appropriate pressure gradient as,

$$\mathbf{u}^{n+1} = \mathbf{u}^\star - \frac{\Delta t}{\rho_f}\nabla p^{n+\frac{1}{2}} \tag{2.76}$$

Applying the continuity equation at the each time step implies that the velocity field should be divergence free.

$$\nabla\cdot\mathbf{u}^{n+1} = 0. \tag{2.77}$$

Substituting Eq. 2.77 into Eq. 2.76 yields the following Poisson equation for pressure.

$$\nabla \cdot \left[ \frac{\Delta t}{\rho_f} \nabla p^{n+\frac{1}{2}} \right] = \nabla \cdot \mathbf{u}^{\star}. \tag{2.78}$$

Finally the velocity at the next time step can be obtained from Eq. 2.76

### 2.3.2 Spatial Discretization

### 2.3.3 Advection Term

The advection term $\mathbf{u}^{n+\frac{1}{2}} \nabla \mathbf{u}^{n+\frac{1}{2}}$ is discretized using the second order Godunov approach proposed by Bell et al. [44]. The advection term at cell centers can be written based on the fluxes at the cell faces.

$$\int_C \mathbf{u}^{n+\frac{1}{2}} \cdot \nabla \mathbf{u}^{n+\frac{1}{2}} = \int_C \nabla \cdot [\mathbf{u}\mathbf{u}]^{n+\frac{1}{2}} = \oint_f \mathbf{u}_f^{n+\frac{1}{2}} (\mathbf{u}_f^{n+\frac{1}{2}} \cdot \mathbf{n}_f) \tag{2.79}$$

which for Cartesian grids can be written as,

$$\Delta x \left( \mathbf{u}^{n+\frac{1}{2}} \cdot \nabla \mathbf{u}^{n+\frac{1}{2}} \right) = \sum_f \mathbf{u}_f^{n+\frac{1}{2}} u_f^{n+\frac{1}{2}} \tag{2.80}$$

where $\mathbf{u}^{n+\frac{1}{2}}$ is the velocity at the center of the face and $u_f^{n+\frac{1}{2}}$ is the normal component of the velocity at the face centers.

In order to approximate face centered values at the time $n + \frac{1}{2}$ we use the Taylor series expansion as,

$$\begin{aligned}
u_{i+\frac{1}{2},j}^{n+\frac{1}{2},L} &= u_{i,j}^n + \frac{\Delta x}{2} \frac{\partial u_{i,j}^n}{\partial x} + \frac{\Delta t}{2} \frac{\partial u_{i,j}^n}{\partial t} \\
u_{i-\frac{1}{2},j}^{n+\frac{1}{2},R} &= u_{i,j}^n - \frac{\Delta x}{2} \frac{\partial u_{i,j}^n}{\partial x} + \frac{\Delta t}{2} \frac{\partial u_{i,j}^n}{\partial t} \\
u_{i,j+\frac{1}{2}}^{n+\frac{1}{2},B} &= u_{i,j}^n + \frac{\Delta y}{2} \frac{\partial u_{i,j}^n}{\partial y} + \frac{\Delta t}{2} \frac{\partial u_{i,j}^n}{\partial t} \\
u_{i,j-\frac{1}{2}}^{n+\frac{1}{2},T} &= u_{i,j}^n - \frac{\Delta y}{2} \frac{\partial u_{i,j}^n}{\partial y} + \frac{\Delta t}{2} \frac{\partial u_{i,j}^n}{\partial t}
\end{aligned}$$

superscripts $L$, $R$, $B$, $T$, indicate the extrapolation of $\mathbf{u}_{ij}$ to the left, right, bottom, and top edges of the cell. The temporal derivative can be substituted by spatial derivative using Euler equation.

$$u_{i+\frac{1}{2},j}^{n+\frac{1}{2},L} = u_{i,j}^n + \left[ \frac{\Delta x}{2} - \frac{\Delta t}{2} v_{i,j}^n \right] \frac{\partial u_{i,j}^n}{\partial x} + \frac{\Delta t}{2} v_{i,j}^n \frac{\partial u_{i,j}^n}{\partial t} - \frac{\Delta t}{2} \nabla p_{i,j}^n \tag{2.81}$$

Normal derivatives are evaluated using the limited slopes whereas transverse derivatives are treated in an upwind manner as follows,

$$\frac{\partial u_{i,j}}{\partial y} = \frac{u_{i,j} - u_{i,j-1}}{\Delta y} + \frac{1}{2}\left(1 - \frac{\Delta t v_{i,j}}{\Delta y}\right)\frac{D_y u_{i,j} - D_y u_{i,j-1}}{\Delta y}, \quad v_{i,j} > 0$$
$$\frac{\partial u_{i,j}}{\partial y} = \frac{u_{i,j+1} - u_{i,j}}{\Delta y} - \frac{1}{2}\left(1 + \frac{\Delta t v_{i,j}}{\Delta y}\right)\frac{D_y u_{i,j+1} - D_y u_{i,j}}{\Delta y}, \quad v_{i,j} < 0$$

where $D_y$ represents central differencing operator. Finally approximation for advection term, $\mathbf{u}^{n+\frac{1}{2}}\nabla\mathbf{u}^{n+\frac{1}{2}}$ can be written in the following discretized form.

$$\begin{aligned}\mathbf{u}^{n+\frac{1}{2}}\nabla\cdot\mathbf{u}^{n+\frac{1}{2}} = \Bigg[&\frac{u_{i+\frac{1}{2},j}\mathbf{u}_{i+\frac{1}{2},j} - u_{i-\frac{1}{2},j}\mathbf{u}_{i-\frac{1}{2},j}}{\Delta x} + \frac{v_{i,j+\frac{1}{2}}\mathbf{u}_{i,j+\frac{1}{2}} - v_{i,j-\frac{1}{2}}\mathbf{u}_{i,j-\frac{1}{2}}}{\Delta y}\\ &- \frac{1}{2}(\mathbf{u}_{i+\frac{1}{2},j} + \mathbf{u}_{i-\frac{1}{2},j})\frac{u_{i+\frac{1}{2},j} - u_{i-\frac{1}{2},j}}{\Delta x}\\ &- \frac{1}{2}(\mathbf{u}_{i,j+\frac{1}{2}} + \mathbf{u}_{i,j-\frac{1}{2}})\frac{v_{i,j+\frac{1}{2}} - v_{i,j-\frac{1}{2}}}{\Delta y}\Bigg]^{n+\frac{1}{2}}\end{aligned}$$

which can be further simplified to the following form,

$$\begin{aligned}\mathbf{u}^{n+\frac{1}{2}}\nabla\cdot\mathbf{u}^{n+\frac{1}{2}} = \Bigg[&\frac{1}{2}(u_{i+\frac{1}{2},j} + u_{i-\frac{1}{2},j})\frac{\mathbf{u}_{i+\frac{1}{2},j} - \mathbf{u}_{i-\frac{1}{2},j}}{\Delta x}\\ &+ \frac{1}{2}(v_{i,j+\frac{1}{2}} + v_{i,j-\frac{1}{2}})\frac{\mathbf{u}_{i,j+\frac{1}{2}} - \mathbf{u}_{i,j-\frac{1}{2}}}{\Delta y}\Bigg]^{n+\frac{1}{2}}\end{aligned}$$

### 2.3.4 Projection

In order to make our computed face center velocity field divergence free we need to solve Eq.2.77 equation. In this equation the right hand side is calculated at each grid cells as,

$$\nabla\cdot\mathbf{u}^{\star}_{i,j} = \frac{u^{\star}_{i+\frac{1}{2},j} - u^{\star}_{i-\frac{1}{2},j}}{\Delta x} + \frac{v^{\star}_{i,j+\frac{1}{2}} - v^{\star}_{i,j-\frac{1}{2}}}{\Delta y}. \tag{2.82}$$

Then using the iterative methods we solve the resulting Poisson equation.

$$\nabla\cdot\left(\frac{\Delta t}{\rho_f}\nabla p_{i,j}\right) = \nabla\cdot\mathbf{u}^{\star}_{i,j}. \tag{2.83}$$

We update the face centered velocity field by adding the pressure differences as,

$$u^{n+1}_{i+\frac{1}{2},j} = u^{\star}_{i+\frac{1}{2},j} - \frac{\Delta t}{\rho_{i+\frac{1}{2},j}}\left(\frac{p_{i+1,j} - p_{i,j}}{\Delta x}\right) + \frac{\Delta t}{\rho_{i+\frac{1}{2}}}\mathbf{F}_{i+\frac{1}{2},j}$$
$$u^{n+1}_{i-\frac{1}{2},j} = u^{\star}_{i-\frac{1}{2},j} - \frac{\Delta t}{\rho_{i-\frac{1}{2},j}}\left(\frac{p_{i,j} - p_{i-1,j}}{\Delta x}\right) + \frac{\Delta t}{\rho_{i-\frac{1}{2}}}\mathbf{F}_{i-\frac{1}{2},j}.$$

### 2.3.5 Viscous Term

The integral of viscous fluxes at the cell faces can be spatially discretized as,

$$(D_x)_{i+\frac{1}{2},j} = \frac{\mathrm{T}^{xx}_{i+1,j} - \mathrm{T}^{xx}_{i,j}}{\Delta x} + \frac{\mathrm{T}^{xy}_{i+\frac{1}{2},j+\frac{1}{2}} - \mathrm{T}^{xy}_{i+\frac{1}{2},j-\frac{1}{2}}}{\Delta y} \tag{2.84}$$

$$(D_y)_{i,j+\frac{1}{2}} = \frac{\mathrm{T}^{yy}_{i,j+1} - \mathrm{T}^{yy}_{i,j}}{\Delta y} + \frac{\mathrm{T}^{xy}_{i+\frac{1}{2},j+\frac{1}{2}} - \mathrm{T}^{xy}_{i-\frac{1}{2},j+\frac{1}{2}}}{\Delta x}. \tag{2.85}$$

where $\mathrm{T}^{yy}$, $\mathrm{T}^{xy}$, $\mathrm{T}^{xx}$ are viscous stress tension components. Using second order central differentiating, viscous stress tension components can be written as,

$$\mathrm{T}^{xx}_{i,j} = \mu^n_{i,j}\frac{u^n_{i+\frac{1}{2},j} - u^n_{i-\frac{1}{2},j}}{\Delta x}, \tag{2.86}$$

$$\mathrm{T}^{xy}_{i+\frac{1}{2},j+\frac{1}{2}} = \mu^n_{i+\frac{1}{2},j+\frac{1}{2}}\left(\frac{u^n_{i+\frac{1}{2},j+1} - u^n_{i+\frac{1}{2},j}}{\Delta y} + \frac{v^n_{i+1,j+\frac{1}{2}} - v^n_{i,j+\frac{1}{2}}}{\Delta x}\right), \tag{2.87}$$

$$\mathrm{T}^{yy}_{i,j} = \mu^n_{i,j}\frac{v^n_{i,j+\frac{1}{2}} - u^n_{i,j-\frac{1}{2}}}{\Delta y}, \tag{2.88}$$

### 2.3.6 Two-Phase Flows

Sussman et al. [38] proposed a level-set model for simulation of two-phase flows. In this model we use the Navier-Stokes equations represented in Section. 2.3 to simulate fluids behavior on the both sides of the interface.

$$\rho\frac{\partial \mathbf{u}}{\partial t} + \rho\mathbf{u}\cdot\nabla\mathbf{u} = -\nabla p + \nabla\cdot(2\mu\mathbf{D}) + \mathbf{F}_b. \tag{2.89}$$

where $\rho$, and $\mu$ are not spatially constant. Generally in two-phase flows properties of fluids are different and there is a jump at the interface in properties of the fluids. The following relations can be used to define properties throughout the whole domain.

$$\rho(\phi) = \rho^- + \left(\rho^+ - \rho^-\right)H(\phi), \tag{2.90}$$

$$\mu(\phi) = \mu^- + \left(\mu^+ - \mu^-\right) H(\phi), \tag{2.91}$$

where $\rho^-$, $\rho^+$, $\mu^+$, and $\mu^-$ represent densities and viscosities in each phase. $H(\phi)$ is Heaviside function define as

$$H(\phi) = \begin{cases} 1 & \phi > 0 \\ 0 & \phi < 0 \end{cases} \tag{2.92}$$

This equation to define properties may induce discontinuities at the interface. The jump at the interface may cause several numerical issues specially when difference between properties is large. In order to alleviate the discontinuity of properties in two-phase flows we use smeared-out functions to define properties throughout the whole domain. Sussman et al. [38] proposed the following smeared-out Heaviside function to avoid sharp jumps at the interface.

$$H_\epsilon(\phi) = \begin{cases} 0 & \phi < -\epsilon \\ \frac{1}{2} + \frac{\phi}{2\epsilon} + \frac{1}{2\pi}\sin\left(\frac{\pi\phi}{\epsilon}\right) & -\epsilon \leq \phi \leq \epsilon \\ 1 & \epsilon < \phi \end{cases} \tag{2.93}$$

where $\epsilon$ can be chosen as $1.5\Delta x$ which makes the interface width equal to three grid cells. In certain situations we need to define fluid properties at cell faces instead of cell centers. In order to approximate face centered values we have two options. First we can use simple averaging of cell centered values as,

$$\rho_{i+\frac{1}{2},j} = \frac{\rho_{i,j} + \rho_{i+1,j}}{2}. \tag{2.94}$$

However, we use a more accurate approach for approximation of face centered values using the following equation.

$$\rho(\phi) = \rho^- + \left(\rho^+ - \rho^-\right) H_\epsilon(\phi_{i+\frac{1}{2}}), \tag{2.95}$$

where $H_\epsilon$ is smeared-out Heaviside function and $\phi_{i+\frac{1}{2}}$ is the value of level set function at the cell faces, defined by

$$\phi_{i+\frac{1}{2},j} = \frac{\phi_{i,j} + \phi_{i+1,j}}{2}. \tag{2.96}$$

### 2.3.7 Pressure Jump

One of the most important aspect of multiphase flows is dealing with pressure jump at the liquid-gas interfaces resulting from surface tension forces. The Laplace's relation between pressure and surface tension can be expressed as,

$$[p] = \sigma\kappa \tag{2.97}$$

where $[p]$ represents the jump of the pressure across the interface and $\sigma$ is liquid surface tension coefficient, and $\kappa$ is curvature. There are various approaches in the literature to evaluate pressure jumps. In the first approach the surface tension forces are added as volumetric source term in momentum equation. If we set $\mathbf{u} = 0$ in Navier-Stokes equations, we get the following equilibrium condition.

$$-\nabla p + \sigma\kappa\mathbf{n}\delta_\epsilon = 0, \tag{2.98}$$

where $\delta_\epsilon$ is smeared-out delta function defined as,

$$\delta_\epsilon(\phi) = \begin{cases} 0 & \phi < -\epsilon \\ \frac{1}{2\epsilon} + \frac{1}{2\epsilon}\cos\left(\frac{\pi\phi}{\epsilon}\right) & -\epsilon \leq \phi \leq \epsilon \\ 0 & \epsilon < \phi \end{cases} \tag{2.99}$$

where $\epsilon = 1.5\Delta x$. In the context of level-set method curvature, $\kappa$, can be evaluated as,

$$\mathbf{n} = \frac{\nabla\phi}{|\nabla\phi|} \quad \text{and} \quad \kappa = \nabla \cdot \mathbf{n}. \tag{2.100}$$

which represents the curvature of the local contour of the level-set and defines the curvature everywhere in the domain, not just at the interface. An accurate estimation of curvature is centeral to the performance of volumetric surface tension force model. A simple discretization of curvature equation can be performed using the following relation.

$$\kappa_{i+\frac{1}{2},j} = \frac{\kappa_{i,j} + \kappa_{i+1,j}}{2}. \tag{2.101}$$

where $\kappa_i$ is evaluated at cell centers as,

$$\kappa_i = \left(\nabla \cdot (\nabla\phi)_f\right), \tag{2.102}$$

However using this naive discretization may result in a curvature field that is not constant across the interface which consequently will lead to violation of the Laplace's equilibrium condition. An improved version of curvature approximation is proposed by Fedkiw et al. [45] as,

$$\kappa_{i+\frac{1}{2}} = \frac{\kappa_i|\phi_{i+1}| + \kappa_{i+1}|\phi_i|}{|\phi_i| + |\phi_{i+1}|} \tag{2.103}$$

which provides better and more accurate approximation of curvature.

Another approach to deal with surface tension forces at liquid gas interfaces is to impose the pressure jump directly in the pressure projection equation. In this approach we use the GFM to solve variable coefficient Poisson equation with jump condition at

the interface.

$$\nabla \cdot (\beta \nabla p) = f, \tag{2.104}$$

$$[p] = a, \tag{2.105}$$

$$[\beta p_n] = b \tag{2.106}$$

where in the context of pressure correction $\beta = \frac{1}{\rho}$, and $a = \sigma\kappa$, and for simplicity we can assume that the $b = 0$ . The one dimensional second order discretization of the equation without jump at the interface can be written as,

$$\frac{\beta_{i+\frac{1}{2}} \left( \frac{a_{i+1} - a_i}{\Delta x} \right) - \beta_{i-\frac{1}{2}} \left( \frac{a_i - a_{i-1}}{\Delta x} \right)}{\Delta x} = f_i \tag{2.107}$$

which can be written for each unknown $p_i$. Assume that interface is located between $x_k$ and $x_{k+1}$. We discretize the jump condition $[\beta p_x] = b$ as,

$$\beta^+ \left( \frac{p_{k+1} - p_I}{(1-\theta)\Delta x} \right) - \beta^- \left( \frac{p_I - p_k}{\theta \Delta x} \right) = b \tag{2.108}$$

by solving the equation for $p_I$ we have

$$p_I = \frac{\beta^+ p_{k+1} \theta + \beta^- p_k (1-\theta) - b\theta(1-\theta)\Delta x}{\beta^+ \theta + \beta^- (1-\theta)}, \tag{2.109}$$

so that left and right side derivatives can be approximated as,

$$\beta^+ \left( \frac{p_{k+1} - p_I}{(1-\theta)\Delta x} \right) = \hat{\beta} \left( \frac{p_{k+1} - p_k}{\Delta x} \right) + \frac{\hat{\beta} b \theta}{\beta^-}, \tag{2.110}$$

$$\beta^+ \left( \frac{p_I - p_k}{\theta \Delta x} \right) = \hat{\beta} \left( \frac{p_{k+1} - p_k}{\Delta x} \right) - \frac{\hat{\beta} b (1-\theta)}{\beta^+}, \tag{2.111}$$

where $\hat{\beta}$ represents an effective $\beta$ defined as,

$$\hat{\beta} = \frac{\beta^+ \beta^-}{\beta^+ \theta + \beta^- (1-\theta)} \tag{2.112}$$

By substituting it into the Poisson equation we obtain the following symmetric linear equation.

$$\frac{\beta_{i+\frac{1}{2}} \left( \frac{p_{i+1} - p_i}{\Delta x} \right) - \beta_{i-\frac{1}{2}} \left( \frac{p_i - p_{i-1}}{\Delta x} \right)}{\Delta x} = f_i + F_L + F_R \tag{2.113}$$

where $\beta_{i+\frac{1}{2}}$ is evaluated based on the interface location. If interface is located between $x_k$ and $x_{k+1}$, $F_L = 0$ and $F_R$ is evaluated as,

$$F_R = -\frac{\hat{\beta}a}{(\Delta x)^2} + \frac{\hat{\beta}b\theta}{\beta^- \Delta x} \tag{2.114}$$

where the effective $\beta$ is evaluated from Eq.2.112, and $\theta$ is obtained from

$$\theta = \frac{|\phi_{i-1}|}{|\phi_i| + |\phi_{i-1}|}. \tag{2.115}$$

On the other hand if interface $x_\Gamma$ is located between $x_i$ and $x_{i-1}$ the $F_R$ will be zero and $F_L$ can be obtained as

$$F_L = \frac{\hat{\beta}a}{(\Delta x)^2} + \frac{\hat{\beta}b(1-\theta)}{\beta^+ \Delta x} \tag{2.116}$$

where $\theta$ is calculated as,

$$\theta = \frac{|\phi_{i+1}|}{|\phi_i| + |\phi_{i+1}|}. \tag{2.117}$$

For the sake of simplicity it can be assumed that there is no jump in the value of $\beta p_n$ which implies that $b = 0$. In addition after obtaining pressure from Poisson equation as described above one needs to correct velocities by including surface tension force.

## 2.4 Three Phase Liquid Solidification

In this section we describe a new level-set approach for modelling three-phase unconstrained solidification problem by considering the effect of liquid density expansion effect during solidification. The unconstrained solidification problem refers to liquid solidification where the interface of liquid is not confined by a container. In this case the interface of the liquid will be affected by solidification process specially when there is a significant amount of density expansion or shrinkage during freezing process. An example of unconstrained freezing is droplet solidification on cold plates where solidification interface starts to move upward from bottom of the droplet. In the proposed approach, we use two different level-sets for tracking liquid-gas and liquid-solid interfaces. The liquid-gas interface is affected by fluid dynamics while the energy equation and release of latent heat of fusion are governing the solid-liquid interface.

### 2.4.1 Multiple Level-Sets

In the case of three-phase physical problems there are two interface that need to be tracked using an appropriate method. We define two level-sets in the whole domain and associate each interface with a particular phase. As illustrated in Fig. 2.3 the level-

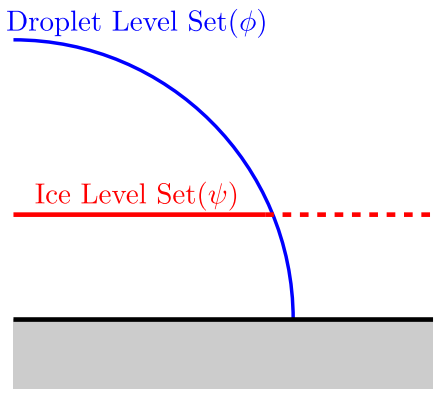


Figure 2.3: Schematic of multiple level-sets for modeling three phase flows.

set $\phi$ represent the interface of liquid-gas and $\psi$ represents the liquid-solid interface. Hence each phase can be distinguished based on the sign of each level-set as,

$$Phase = \begin{cases} Liquid & \phi < 0 \quad \& \quad \psi > 0 \\ Solid & \phi < 0 \quad \& \quad \psi < 0 \\ Gas & \phi > 0 \quad \& \quad \psi > 0 \end{cases} \tag{2.118}$$

Properties are constant in each phase but varying throughout the domain. In order to set properties of each phase we use Heaviside function.

$$C(\mathbf{x}) = (1 - H(\phi))C_{Solid} + H(\phi)(1 - H(\psi))C_{Liquid} + H(\phi)H(\psi)C_{Gas} \tag{2.119}$$

where $C$ can be a property of each phase such as density, viscosity, heat conductivity or heat diffusivity. In order to avoid discontinuities at the interfaces we use smeared-out Heaviside function. The level-set associated with the solidifying interface is divided into two segments: active; passive. The active segment is governed by heat transfer and solidification rate while the passive part only is used for imposing tri-junction angle.

### 2.4.2 Imposing Tri-Junction Angle

The intersection of liquid-solid interface with liquid-gas interface forms a tri-junction point which needs to be treated carefully. At this point there is a discontinuity in the slope of solidifying and droplet interface (Fig. 2.4). Using the model proposed in this study we can implicitly impose the angle between two interfaces as described in this section. Using the fact that the angle between normal to each interface should be equal

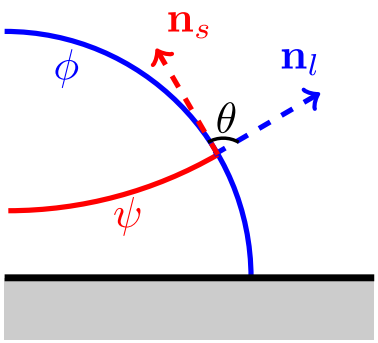


Figure 2.4: Schematic of tri-junction angle.

to the angle of two interfaces, we can write

$$\mathbf{n}_s \cdot \mathbf{n}_l = cos(\theta) \tag{2.120}$$

where $n_s$, $n_l$, and $\theta$ are normal to solid interface, normal to liquid interface, and the angle of solidifying and droplet interfaces. Rewriting normals based on the gradients of level-sets yields,

$$\frac{\nabla\phi}{|\nabla\phi|} \cdot \frac{\nabla\psi}{|\nabla\psi|} = cos(\theta), \tag{2.121}$$

where we only update values of level-sets associated with the solidifying interface. In order to solve this equation we use pseudo-time dependent equation and solve it to reach steady-state condition.

$$\frac{\partial\psi}{\partial t} + \frac{\nabla\phi}{|\nabla\phi|} \cdot \frac{\nabla\psi}{|\nabla\psi|} = cos(\theta) \tag{2.122}$$

Note however that by solving this equation we are updating values of $\psi$ throughout the whole domain which is not desirable. We use smeared-out Heaviside function to restrict updating of $\psi$ where the value of $\phi$ is positive. Hence, the equation can be written as,

$$\frac{\partial\psi}{\partial t} + H_\epsilon(\phi)\frac{\nabla\phi}{|\nabla\phi|} \cdot \frac{\nabla\psi}{|\nabla\psi|} = H_\epsilon(\phi)cos(\theta) \tag{2.123}$$

where $|\nabla\phi|$, $|\nabla\psi|$, and $\nabla\phi$ are discretized using central differencing scheme while for $|\nabla\psi|$ we use upwind differencing scheme based on the sign of $H_\epsilon(\phi)\frac{\nabla\phi}{|\nabla\phi|}$.

### 2.4.3 Poisson Equation

In the proposed three-phase model we need to solve Poisson equation throughout the whole domain while applying fixed value boundary condition on the active segment of moving solidifying front. To this end, we modified the approach explained in Section. 2.2.1. Mathematical expression of Poisson equation with fixed value boundary condition only at active part of the solidifying interface can be written as,

$$\nabla \cdot (\beta \nabla a) = f \tag{2.124}$$

$$T = T_I \quad \text{on} \quad \Gamma_1 \tag{2.125}$$

where $\Gamma_1$ is defined in the active part of the interface. We use the sign of $\phi$ to distinguish active and passive parts of the $\psi$. Discretization of Poisson equation for cells with $\psi > 0$ or cells with $\psi < 0$ that are not in the vicinity of the interface can be written as,

$$\frac{\beta_{i+\frac{1}{2}} \left( \frac{a_{i+1} - a_i}{\Delta x} \right) - \beta_{i-\frac{1}{2}} \left( \frac{a_i - a_{i-1}}{\Delta x} \right)}{\Delta x} = f_i \tag{2.126}$$

otherwise we use either

$$\frac{\beta_{i+\frac{1}{2}} \left( \frac{a_I - a_i}{\theta \Delta x} \right) - \beta_{i-\frac{1}{2}} \left( \frac{a_i - a_{i-1}}{\Delta x} \right)}{\Delta x} = b_i, \quad x_i < x_I < x_{i+1} \tag{2.127}$$

or

$$\frac{\beta_{i+\frac{1}{2}} \left( \frac{a_{i+1} - a_i}{\Delta x} \right) - \beta_{i-\frac{1}{2}} \left( \frac{a_i - a_I}{\theta \Delta x} \right)}{\Delta x} = b_i, \quad x_{i-1} < x_I < x_i. \tag{2.128}$$

Note that using this modification we can impose the fixed value boundary condition at a segment of the interface which is located inside the liquid.

### 2.4.4 Interface Velocity

In three-phase level-set method interface velocity only has meaning in the liquid phase. However, the level-sets associated with the solidifying interface are defined everywhere. Hence, before the extension of the interface velocity using the scheme represented in Section. 2.2.4 we modify interface normal velocity as,

$$v_n = \frac{1}{\rho_l L_H} (1 - H_\epsilon(\phi)) \left[ \kappa_l (\nabla T \cdot \mathbf{n})_l - \kappa_s (\nabla T \cdot \mathbf{n})_s \right] \tag{2.129}$$

where $H_\epsilon$ is smeared-out Heaviside function. This modification results in having interface velocities only in the liquid region. After this step we can extend the interface

velocity by

$$\frac{\partial v_n}{\partial \tau} + S(\phi)\nabla v_n \cdot \mathbf{n} = 0 \tag{2.130}$$

### 2.4.5 Density Variation

During the solidification process there is a density change between the liquid and the solid phases. Some materials such as water expand during solidification. In order to include the density variation in our model we need to find a relationship between the liquid and solidifying interface velocities. To this end, we use the mass conservation law. In an arbitrary control volume that contains both liquid and solid phases the conservation of mass can be written as,

$$\frac{D}{Dt}(M) = 0, \tag{2.131}$$

where $m$ can be written as,

$$M = \int_V \rho dV, \tag{2.132}$$

where $\rho$ is expressed by the following expression,

$$\rho(\mathbf{x}) = \rho_l H(\psi) + \rho_s(1 - H(\psi)). \tag{2.133}$$

By substituting Eq. 2.133 into Eq. 2.132, and writing conservation of mass we obtain

$$\frac{D}{Dt}\int_V [\rho_l H(\psi) + (1 - H(\psi))\rho_s]\, dV = 0. \tag{2.134}$$

Using Reynolds' Transport Theorem and setting zero velocity in the solid phase we have

$$\int_V \left[\frac{\partial}{\partial t}(\rho_l H(\psi)) + \nabla \cdot (\rho_l H(\psi)\mathbf{u_l}) - \frac{\partial}{\partial t}(\rho_s H(\psi))\right] dv = 0, \tag{2.135}$$

that can be rewritten as

$$\nabla \cdot (H(\psi)\mathbf{u_l}) = -\frac{\rho_l - \rho_s}{\rho_l}\frac{\partial}{\partial t}(H(\psi)) \tag{2.136}$$

Using the chain rule and the fact that $\mathbf{u} = \mathbf{u_l}H(\psi) + \mathbf{u_s}(1 - H(\psi))$ we can write

$$\nabla \cdot \mathbf{u} = -\frac{\rho_l - \rho_s}{\rho_l}\frac{\partial}{\partial \psi}(H(\psi))\frac{\partial \psi}{\partial t} \tag{2.137}$$

By definition derivative of Heaviside function is called Delta function which implies

$$\nabla \cdot \mathbf{u} = -\frac{\rho_l - \rho_s}{\rho_l}\delta_\epsilon(\psi)\frac{\partial \psi}{\partial t} \tag{2.138}$$

which can be simplified by substituting time derivative of level-set from level-set advection equation as

$$\nabla \cdot \mathbf{u} = \beta\delta_\epsilon(\psi)v_n|\nabla\psi| \tag{2.139}$$

where $\beta = \frac{\rho_l - \rho_s}{\rho_l}$ and $\delta_\epsilon(\phi)$ is the smeared-out delta function. The parameter $\beta$ represents the volumetric expansion or shrinkage depending on the its sign. Eq. 2.139 is used in the projection step to calculate pressure from intermediate velocity field as

$$\nabla \cdot (\frac{\Delta t}{\rho}\nabla p) = \nabla \cdot \mathbf{u}^* - \beta\delta_\epsilon(\psi)v_n|\nabla\psi| \tag{2.140}$$

Note that the velocity field is divergence free every where in the domain except at the liquid-solid interface. The term $\beta\delta_\epsilon(\psi)v_n|\nabla\psi|$ acts as a source term in the pressure equation which induces negative or positive pressure gradients at the interface. In the proposed three-phase level-set model we multiply the interface velocity by Heaviside function so that the source term is only active inside the droplet creating pressure gradients only at the solidifying interface which is situated inside the droplet.

Asides from mass conservation at the liquid-solid interface we need to impose mass conservation in the liquid phase since in the level-set method there is no explicit mass conservation equation. In general mass of the liquid in a three phase problem can be obtained from:

$$M_l(t) = \int_V (\rho H_\epsilon(\psi)H_\epsilon(-\phi))\, dV \tag{2.141}$$

where $\rho$ is the density of the fluid. The the mass conservation can be written as,

$$\frac{dM_l(t)}{dt} = 0. \tag{2.142}$$

Now by taking the differentiation of Eq. 2.141 with respect to time we have

$$\frac{dM_l(t)}{dt} = \int_V \left(\frac{d\rho}{dt}H_\epsilon(\psi)H(-\phi) + \rho\frac{d(H_\epsilon(\psi))}{dt}H_\epsilon(\phi) + \rho H_\epsilon(\psi)\frac{H_\epsilon(\phi)}{dt}\right) dV \tag{2.143}$$

which can be further simplified as,

$$\frac{dM_l(t)}{dt} = \int_V \left(\frac{d\rho}{dt}H_\epsilon(\psi)H(-\phi) + \rho H_\epsilon(\psi)\delta_\epsilon(\phi)\frac{d\phi}{dt}\right) dV \tag{2.144}$$

by knowing the fact that $\frac{dH_\epsilon(\phi)}{dt} = \frac{dH_\epsilon}{d\phi}\frac{d\phi}{dt}$ and in the advection step the solid interface is not moving which implies that $\frac{d\psi}{dt} = 0$. Furthermore by using the continuity equation of the fluid field

$$\frac{d\rho}{dt} + \nabla \cdot (\rho \mathbf{u}) = 0, \tag{2.145}$$

Eq. 2.144 can be written as

$$\frac{dM_l(t)}{dt} = \int_V \left( -\nabla \cdot (\rho \mathbf{u}) H_\epsilon(\psi) H_\epsilon(-\phi) + \rho H_\epsilon(\psi) \delta_\epsilon(\phi) \frac{d\phi}{dt} \right) dV. \tag{2.146}$$

Then, using $\nabla \cdot (H_\epsilon(-\phi)\rho\mathbf{u}) = \rho\delta_\epsilon \mathbf{u} \cdot \nabla\phi + \nabla \cdot (\rho\mathbf{u}) H_\epsilon(-\phi)$, Eq. 2.146 can be written in the form

$$\frac{dM_l(t)}{dt} = \int_V \left( -\rho\delta_\epsilon(\phi) \left( \frac{\partial \phi}{\partial t} + \mathbf{u} \cdot \nabla\phi \right) + \nabla \cdot (H_\epsilon(\phi)\rho\mathbf{u}) \right) dV. \tag{2.147}$$

The advection equation of level-set with the modification term for mass conservation can be written as

$$\frac{\partial \phi}{\partial t} + \mathbf{u} \cdot \nabla\phi = \zeta(\mathbf{x}, t). \tag{2.148}$$

Since in the level-set advection numerical diffusion is negligible we can assume that $\zeta(t)$ is merely a function of time. Hence by setting $\frac{dM}{dt} = 0$ the Eq. 2.147 can be written as,

$$-\zeta(t) \int_V (\rho\delta_\epsilon(\phi))\, dV + \int_V \nabla \cdot (H_\epsilon(\phi)\rho\mathbf{u}) dV = 0. \tag{2.149}$$

Now the $\zeta(t)$ term can be obtained as,

$$\zeta(t) = \frac{\int_V \nabla \cdot (H_\epsilon(\phi)\rho\mathbf{u}) dV}{\int_V (\rho\delta_\epsilon(\phi))\, dV}. \tag{2.150}$$

By expanding the $\nabla \cdot (H_\epsilon(\phi)\rho\mathbf{u}) = \rho H_\epsilon(\phi) \nabla \cdot \mathbf{u} + \mathbf{u} \cdot \nabla(\rho H_\epsilon(\phi))$ and substituting the term $\nabla \cdot \mathbf{u} = \beta\delta_\epsilon(\phi) v_n |\nabla\psi|$, the modification term can be written as,

$$\zeta(t) = \frac{\int_V (\rho H_\epsilon(\phi) \beta\delta_\epsilon(\phi) v_n |\nabla\psi|)\, dV + \int_V (\rho\delta_\epsilon(\phi)\mathbf{u} \cdot \nabla(\phi))\, dV}{\int_V (\rho\delta_\epsilon(\phi))\, dV}. \tag{2.151}$$

To sum up, in order to impose mass conservation in the liquid phase we use the term $\zeta(t)$ obtained from Eq. 2.151 in the the Eq. 2.148.

In order to take into account the effect of density variation in the heat transfer equation we write the energy balance at the liquid-solid interface as,

$$\rho_l H_l (\mathbf{u}_l - \mathbf{u}_I) \cdot \mathbf{n} - k_l \nabla T \cdot \mathbf{n} = \rho_s H_s (\mathbf{u}_s - \mathbf{u}_I) \cdot \mathbf{n} - k_s \nabla T \cdot \mathbf{n} \tag{2.152}$$

where $H_l = C_{pl}T_m + L_H$ and $H_s = C_{Ps}T_m$ represent enthalpies of liquid and solid, respectively. Rewriting Eq. 2.152 based on the normal interface velocity yields,

$$[\rho_s L_H + (\rho_l C_{Pl} - \rho_s C_{Ps})T_m)]\, v_n = k_s \nabla T \cdot \mathbf{n} - k_l \nabla T \cdot \mathbf{n}. \tag{2.153}$$

which can be further simplified as,

$$\rho_s \hat{L}_H v_n = k_s \nabla T \cdot \mathbf{n} - k_l \nabla T \cdot \mathbf{n}. \tag{2.154}$$

where $\hat{L}_H = L_H + (\rho_l C_{Pl} - \rho_s C_{Ps} Tm)/\rho_s$ represents the effective latent heat of fusion which takes into account the effect of density variation during solidification process.

# Chapter 3

# Validation and Results

In this chapter we use benchmark problems and experimental results in the literature to validate the model presented in Chapter. 2. In the first step we use benchmark problems to validate implementation of two-phase level-set method including re-initialization, advection, velocity extension, and Poisson equation in irregular domains. In the next step, we validate implementation of two-phase Navier-Stokes equations using standard benchmark problems. In addition we use various test cases to validate the proposed model for simulation of three-phase problems with density variation during the phase change process. Finally we present results of droplet solidification process on a flat cold substrate and compare our results with the experimental results in the literature to validate the model.

## 3.1 Level-Set Re-Initialization

The re-initialization of level-sets is of the utmost importance in the accuracy of numerical simulations. In the re-initialization procedure the zero level-set artificially moves which would decrease the volume inside the interface in considerable amount. In the case of solidification this artificial movements of the solidifying interface leads to overestimation of solidification rate. In this section we verify the procedure described in Section. 2.1.3 , using the test case taken from Russo and Smereka [46], to ensure that the interface is not moving during the re-initizalization process. In this problem we have an ellipse as

$$\phi^0(x,y) = f(x,y)\left(\sqrt{\left(\frac{x^2}{A^2}+\frac{y^2}{B^2}\right)}-1\right), \tag{3.1}$$

where

$$f(x,y) = \epsilon + (x-x_0)^2 + (y-y_0)^2, \tag{3.2}$$

and the parameters are given by $A = 0.4$, $B = 0.2$, $\epsilon = 0.01$, $x_0 = 0.35$, and $y_0 = 0.2$. The initial condition for the level-set has both small and large gradients at the vicinity of the interface.

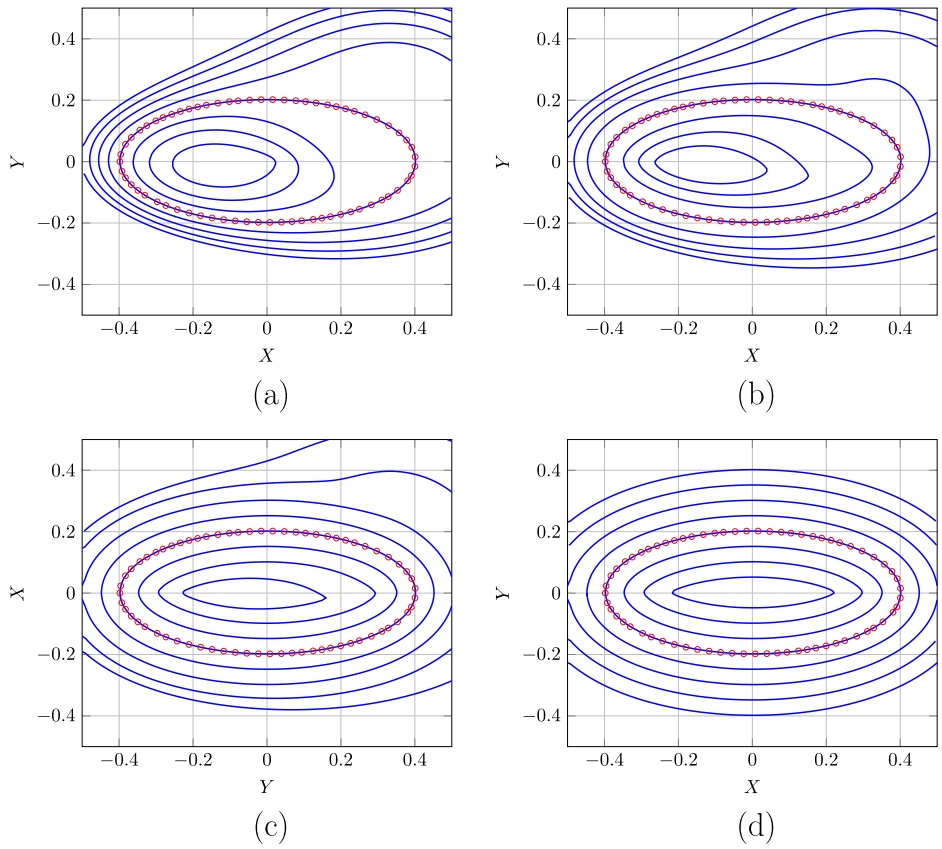


Figure 3.1: Results of re-initialization of level-set method. The domain is $[-0.5, 0.5] \times [-0.5, 0.5]$ and number of cells are 128 in each direction. The number of iterations is a) 0, b) 30, c) 60, d) 90

We use $L^1$ norm of the difference between exact distant function and the computed distant function to validate implementation of numerical methods. The $L^1$ norm can be evaluated as

$$L^1 = \|\phi - \phi_e\| = \sum_{i,j} |\phi_{i,j} - \phi_{ei,j}| \Delta x^2 \tag{3.3}$$

where $\phi_e$ is the exact values of signed distance function from the interface evaluated as

$$\phi_{ei,j} = \min_{0 \le p \le N} |\mathbf{x}_{i,j} - \mathbf{x}_p| Sign(\phi^0_{i,j}), \tag{3.4}$$

where $\mathbf{x_p}$ is the exact location of the interface, and $N$ is number of points on the interface. The interface location, $\mathbf{x_p} = (x_p, y_p)$ , can be calculated as

$$x_p = Acos(\frac{2\pi p}{N}) \tag{3.5}$$

$$y_p = Bsin(\frac{2\pi p}{N}). \tag{3.6}$$

In Fig. 3.1 contours of computed signed distance function in different times are plotted. Note that the location of interface where the value of $\phi$ is zero is not moving. Moreover, the log plot of the $L^1$ error for various grid resolutions are plotted in Fig. 3.2 which implies that the algorithm converges as grid resolution increases. As can be seen in Fig. 3.2 the rate of convergence is between first and second order which can be justified by pointing out that in calculating smeared out sign function we scaled $\epsilon$ as $\Delta x$.

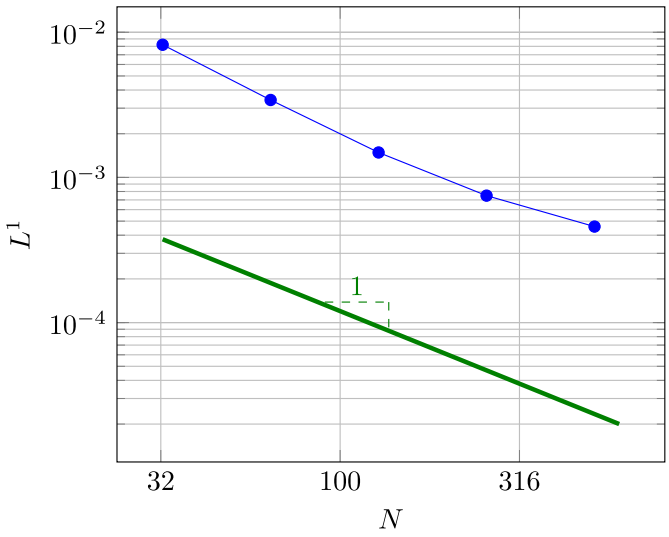


Figure 3.2: $L^1$ error for re-initialization of level-sets against various number of grid cells in each direction.

## 3.2 Advection in Externally Generated Velocity Field

Advection of level-sets under externally generated velocity fields is an important source of errors in multi-phase flows. Inaccurate calculations of gradients in the advection equation may result in mass loss after some time-steps. In this section we assess the performance of the Hamilton-Jabocbi ENO scheme described in Section. 2.1.1 in the

presence of shear flow. In time reversed shear flow benchmark problem which is taken from Rudman [47] the velocity field is given by

$$u(x,y) = \begin{cases} sin(x)cos(y) & 0 \leq t \leq \frac{T}{2} \\ -sin(x)cos(y) & \frac{T}{2} \leq t \leq T \end{cases} \tag{3.7}$$

$$v(x,y) = \begin{cases} -cos(x)sin(y) & 0 \leq t \leq \frac{T}{2} \\ cos(x)sin(y) & \frac{T}{2} \leq t \leq T \end{cases} \tag{3.8}$$

The above velocity field constitutes a time reversed shear flow field defined in the domain $[0,1] \times [0,1]$ which is divided into 128 cells in each direction. A circular interface with the radius of 0.15 is placed in the velocity field centered at $(0.5, 0.25)$. The interface is advected under the shear velocity field such that the interface is largely distorted until the $\frac{T}{2}$. After that the velocity field is reversed to time $T$. Ideally the interface of circle should be the same for times 0 and $T$. However, errors in calculation of gradients may result in error in the position of the interface and possible loss of mass. In Fig. 3.3 results of shear flow advection test case using first order and Hamilton-Jacobi ENO schemes are presented. The solution error is measured in terms of difference between initial and final interfaces which is presented by Sussman and Fatemi [48]. The error measure is given by

$$E_\phi = \frac{1}{L} \sum |H_\epsilon(\phi_i) - H_\epsilon(\phi_f)| \Delta x^2 \tag{3.9}$$

where $L$ is the perimeter of the initial interface, $\phi_i$ is level set field, $\phi_f$ is the final level-set field, and $H_\epsilon$ is the smeared out Heaviside function. This error measures the amount of mass loss during the advection. A summary of errors for various grid resolutions can be find in Table. 3.1. The order of convergence is between first order and second order because we used a combination of HJ-ENO and Runge-Kutta schemes. In order to achieve higher order accuracies HJ-WENO scheme should be employed.

Table 3.1: Summary of errors for advection of a circle under an externally generated velocity field using HJ-ENO Scheme

| Number of Cells | $E_\phi - Error$ | Order |
|---|---|---|
| $32 \times 32$ | $2.8 \times 10^{-2}$ | - |
| $64 \times 64$ | $8.1 \times 10^{-3}$ | 1.8 |
| $128 \times 128$ | $3.4 \times 10^{-3}$ | 1.3 |
| $256 \times 256$ | $1.3 \times 10^{-3}$ | 1.4 |

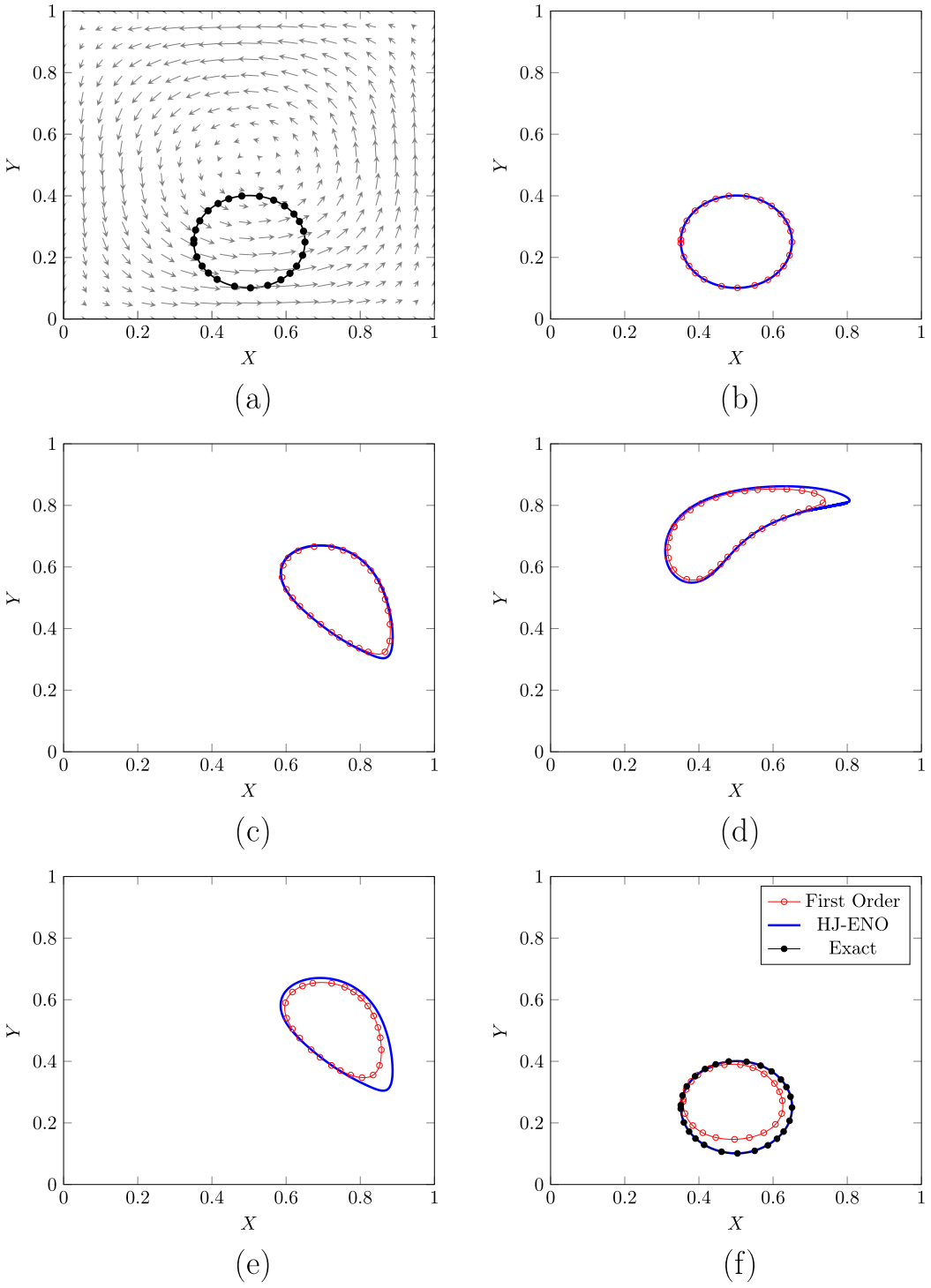


Figure 3.3: Results of advection of a circle in the presence of externally generated shear velocity field at various times b) 0, c) $\frac{T}{4}$, d) $\frac{T}{2}$, e) $\frac{3T}{2}$, f) $T$

## 3.3 Advection in Normal Direction

In numerical modelling of solidification process the solidifying interface is moving under a normal velocity. An accurate method for advection of interface should be able to deal with complicated interfaces. We use evolution of a star shaped geometry to demonstrate that the method described in Section. 2.1.2 can deal with the complicated shapes. The initial level-set is defined as,

$$\phi_0 = \sqrt{(x - x_0)^2 + (y - y_0^2)} - (A + Bsin(N\theta)) \tag{3.10}$$

where $A = 0.5$ and $B = 0.2$ are constant and $N = 7$ determines the number of arms of the star. The normal velocity of the interface is assumed to be $v_n = 1$. The results of the interface at different times for grid resolution of $128 \times 128$ are shown in Fig. 3.4

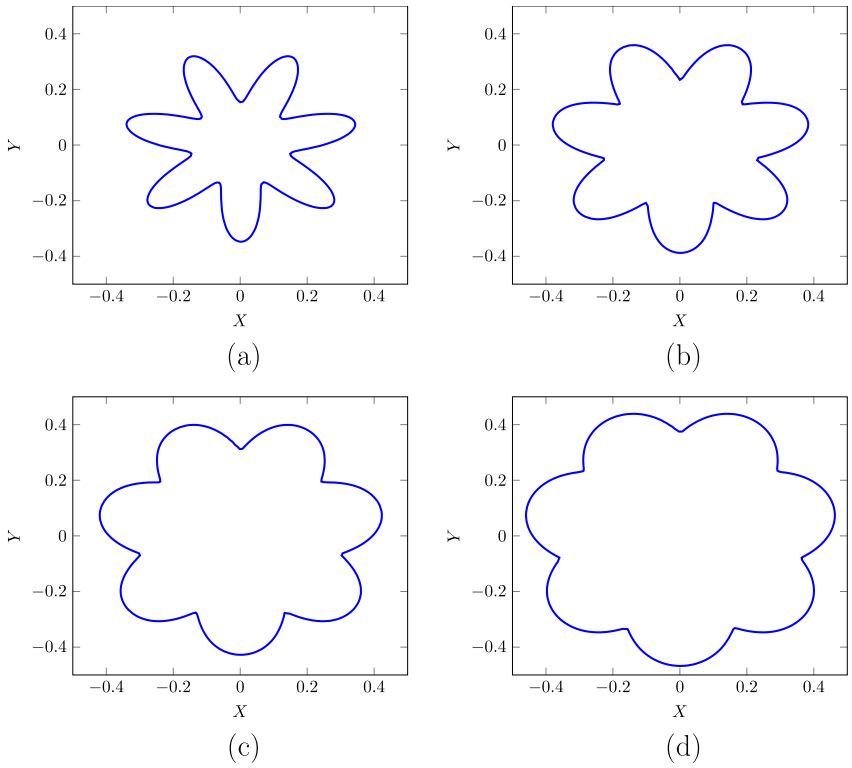


Figure 3.4: Evolution of a star-shaped interface which moves outward in the normal direction after a) 0, b) 0.03, c) 0.06, and d) 0.09s

Moreover, in order to measure the errors associated with the advection of level-set method under normal velocity we used a simple circle which is evolving under constant normal velocity. The area of the region enclosed by the interface can be computed by

$$A(t) = \int_\Omega H_\epsilon(\phi(\mathbf{x}, t))dA \tag{3.11}$$

where the integral is carried out over the whole domain. The numerical estimation of the integral can be written as,

$$A(t) = \sum_i \sum_j H_\epsilon(\phi_{i,j}) \delta x \delta y. \tag{3.12}$$

The error based on the area can be written as

$$E_A = \frac{|A_{exact} - A_{numerical}|}{A_{exact}} \tag{3.13}$$

A summary of Area loss errors for advection of circular interface under normal velocity field can be found in Table. 3.2. Similar to advection under externally generated velocity fields the order of accuracy is between one and two which is expected for the schemes used in this study.

Table 3.2: Summary of errors for advection of a circle under normal velocity field ($v_n = 1$) measured at $t = 0.1s$.

| Number of Cells | $E_A - Error$ | Order |
|---|---|---|
| $32 \times 32$ | $8.1 \times 10^{-3}$ | - |
| $64 \times 64$ | $2.8 \times 10^{-3}$ | 1.5 |
| $128 \times 128$ | $1.2 \times 10^{-3}$ | 1.2 |
| $256 \times 256$ | $5.6 \times 10^{-4}$ | 1.1 |

## 3.4 Poisson Equation in Irregular Domains

In level-set approach, solving Poisson equation on irregular domains is of the crucial importance. In problems including solidification front we need to deal with a moving interface where the Dirichlet boundary conditions for some variables should be applied. The method proposed by Gibou et al. [41] can accurately impose boundary conditions at irregular interfaces. In order to examine implementation of the method presented in Section. 2.2.1 we use the test case represented by Gibou et al. [41]. In this benchmark problem we solve the Poisson equation,

$$\nabla \cdot (\beta \nabla u) = f, \quad \text{in} \quad \Omega \tag{3.14}$$

$$u = g(x,y) \quad \text{on} \quad \Gamma \tag{3.15}$$

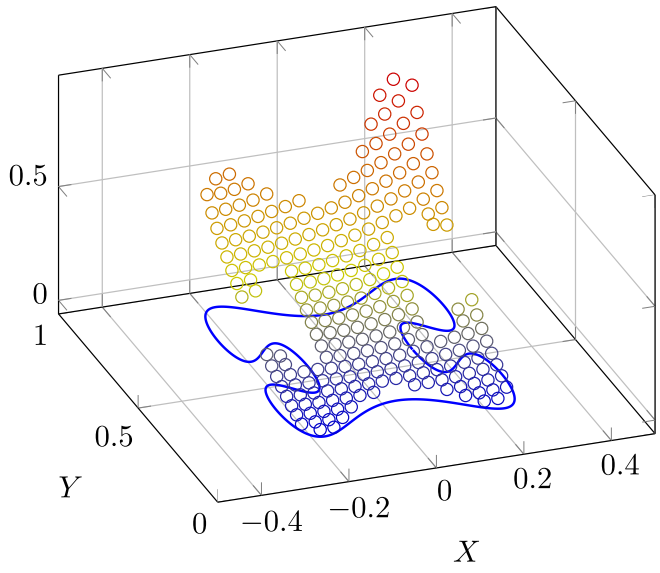


Figure 3.5: Solution of Poisson equation on irregular domain

where $\Gamma$ is the interface defined by the parametric curve as,

$$x(\theta) = 0.3cos(\theta) - 0.15cos(3\theta) \tag{3.16}$$

$$y(\theta) = 0.75 + 0.35sin(\theta) - 0.035sin(3\theta) + 0.1sin(7\theta) \tag{3.17}$$

where $0 \leq \theta \leq < 2\pi$. The exact solution is defined only in the interior region of the interface, $\Omega^-$, as

$$u_e(x,y) = e^x(x^2 sin(y) + y^2) \tag{3.18}$$

hence the source term, $f$, can be determined accordingly,

$$f = \beta^- e^x(2 + y^2 + 2sin(y) + 4xin(y)) \quad \text{if} \quad (x,y) \in \Omega^- \tag{3.19}$$

where $\beta$ is a constant coefficient throughout the domain. The results are showed in Fig. 3.5.

The boundary condition on the boundary interface are obtained from the exact solution of the problem. As can be seen in Fig.3.5 Dirichlet boundary condition is applied on the boundaries. In order to measure the errors we use $L^1$ norm defined as,

$$L^1 = \sum |u_e(\mathbf{x}) - u_c(\mathbf{x})| \tag{3.20}$$

where the $u_e$ and $u_c$ represent exact and computed fields. $L^1$ errors of Poisson equation are summarized in Table. 3.3. As can be seen in Table. 3.3 numerical results converge with second order accuracy. Since we use liner interpolation of ghost values near the interface a small drop in the order of accuracy is expected.

Table 3.3: Summary of errors for solution of Poisson equation inside an irregular domain

| Number of Cells | $L^1 - Error$ | Order |
|---|---|---|
| $32 \times 32$ | $9.1 \times 10^{-4}$ | - |
| $64 \times 64$ | $2.3 \times 10^{-4}$ | 1.9 |
| $128 \times 128$ | $7.1 \times 10^{-5}$ | 1.7 |
| $256 \times 256$ | $2.1 \times 10^{-5}$ | 1.8 |

## 3.5 Heat Equation in Irregular Domains

In this section we use the approach presented in Section. 2.2.2 to solve heat equation which is taken from Gibou et al. [41]

$$\frac{\partial T}{\partial t} = \nabla \cdot (\hat{k} \nabla u), \quad \text{in} \quad \Omega^- \tag{3.21}$$

$$u = g(x,y) \quad \text{on} \quad \Gamma \tag{3.22}$$

where $\Gamma$ is a star with 5 arms defined by

$$x(\theta) = 0.5 + 0.2sin(5\theta)cos(\theta) \tag{3.23}$$

$$y(\theta) = 0.5 + 0.2sin(5\theta)sin(\theta) \tag{3.24}$$

with $\theta \in [0, 2\pi]$. The exact solution is represented by

$$T_e(x,y) = e^{-2t} sin(x) sin(y) \tag{3.25}$$

Solution of the heat equation is shown in Fig.3.6. Similar to Poisson equation we use $L^1$ norm to measure the errors.

$$L^1 = \sum |T_e(\mathbf{x}) - T_c(\mathbf{x})| \tag{3.26}$$

where the $T_e$ and $T_c$ represent exact and computed fields. $L^1$ errors for various grid resolutions at final time are presented in Table. 3.4. Similar to solution of Poisson equation in irregular domains we expect to have a second order accuracy which can be seen in Table. 3.4. Since we use linear interpolations near the interface the accuracy is smaller than second order.

Table 3.4: Summary of errors for solution of Heat equation inside an irregular domain at $t = 0.1s$

| Number of Cells | $L^1 - Error$ | Order |
|---|---|---|
| $32 \times 32$ | $1.3 \times 10^{-3}$ | - |
| $64 \times 64$ | $4.3 \times 10^{-4}$ | 1.6 |
| $128 \times 128$ | $1.2 \times 10^{-4}$ | 1.8 |
| $256 \times 256$ | $3.1 \times 10^{-5}$ | 1.9 |

## 3.6 Stefan Problem

We use classical Stefan problem to validate solidification rate calculations. The governing equations for 1D Stefan problem are represented as,

$$\frac{\partial T}{\partial t}(x,t) = \frac{\partial}{\partial x}\left(k_l \frac{\partial T}{\partial x}\right), \quad x \quad \in \Omega_l(t) \tag{3.27}$$

$$\frac{\partial T}{\partial t}(x,t) = \frac{\partial}{\partial x}\left(k_s \frac{\partial T}{\partial x}\right), \quad x \quad \in \Omega_s(t) \tag{3.28}$$

where $k_{liq}$, and $k_{sol}$ denote the thermal diffusivity in the solid and the liquid phases, respectively. In this problem we assume that these properties are constant in each phase.

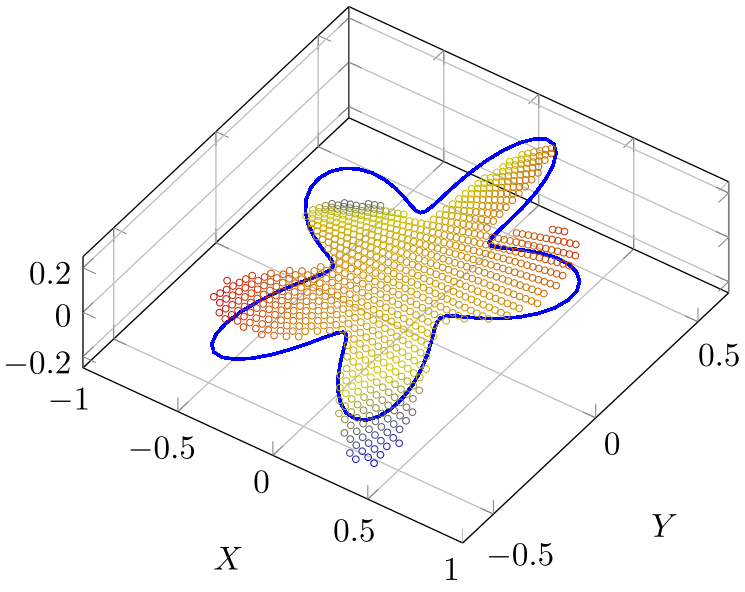


Figure 3.6: Solution of heat equation on irregular domain at time at $t = 0.1$ with 128 gird cells in each direction.

The velocity of the interface is calculated from the following relation.

$$L_H v_n = k_s \frac{\partial T}{\partial x} - k_l \frac{\partial T}{\partial x} \tag{3.29}$$

where $L_H$ represents th latent heat of fusion. The temperature of the interface is set to zero

$$T(s(t), t) = 0, \tag{3.30}$$

where $s(t)$ is location of the interface. The solution of this problem can be expressed in the form of

$$s(t) = s_0(t) + 2\alpha\sqrt{t}, \tag{3.31}$$

where the constant $\alpha$ is obtained by solving the following equation.

$$\alpha = \frac{\sqrt{k_l}}{\sqrt{\pi L_H}} \frac{T_s}{erfc(\frac{\alpha}{\sqrt{k_s}})} exp(-\frac{\alpha^2}{k_s}) + \frac{\sqrt{k_l}}{\pi L} \frac{T_l}{\sqrt{\pi L}} \frac{T_l}{2 - erfc(\frac{\alpha}{\sqrt{k_l}})} exp(-\frac{\alpha^2}{k_l}), \tag{3.32}$$

while the temperature can be calculated as,

$$T(\mathbf{x}, t) \begin{cases} -\frac{T_l erfc(\alpha/\sqrt{k_l})}{2 - erfc(\alpha/\sqrt{k_l})} + \frac{T_l erfc((x - s_0)/2\sqrt{k_l t})}{2 - erfc(\alpha/\sqrt{k_l})}, & if x < s(t) \\ T_s - \frac{T_s erfc((x - s_0)/2\sqrt{k_s t})}{erf(\alpha/\sqrt{k_s})}, & of x \geq s(t) \end{cases} . \tag{3.33}$$

Numerical results of level-set method compared with the analytical solution is plotted in Fig. 3.7 for $L_H = 0.53$ and $k = 1$ for both phases. The convergence of the solution by grid resolution plotted in Fig. 3.7(c) reveals that the numerical method has first order convergence. The first order convergence of Stafan problem is because we approximate gradients of temperature using first order accurate method which consequently results in a first order prediction of interface velocities. Note that the temperature at the interface is set to zero.

## 3.7 Pressure Jump

The accurate estimation of the surface tension forces in the Navier-Stokes equations has proven to be one of the most difficult aspects of the surface tension driven flows. Laplace balance between surface tension force and pressure gradient at the interface of two phase flows is difficult to reproduce numerically which leads to production of so-called spurious currents. In order to reduce the spurious currents at the interface one needs to accurately treat the pressure jump and force balance at the interface. Using the ghost fluid method described in Section.2.3.7 it is possible to accurately treat the surface tension forces at the interface. In order to validate numerical methods for solving

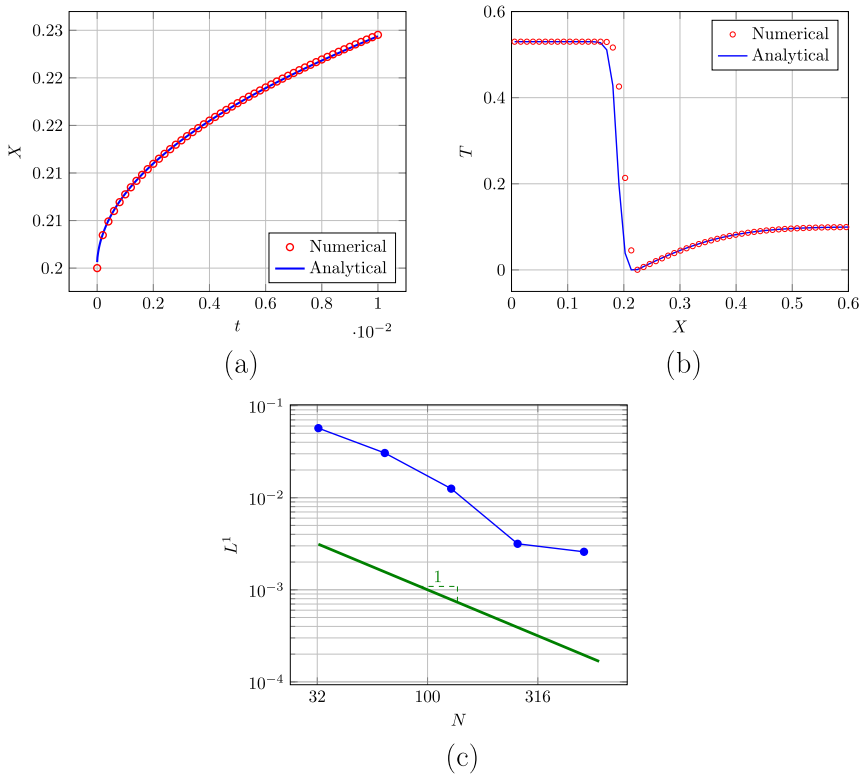


Figure 3.7: One dimensional Stefan problem using level-set method. a) Interface position v. s time; b) Temperature field; c) Spatial convergence of interface location

pressure equation in the case of jump condition at the interface we consider a stationary droplet with the interface defined as

$$\phi(x,y) = \sqrt{x^2 + y^2} - R_0 \tag{3.34}$$

where $R_0 = 0.5$ is the radius of the circle. We can describe the problem using the Poisson equation with jump at the interface as,

$$\nabla \cdot (\nabla P) = 0, \tag{3.35}$$

$$[P] = 1. \quad \mathbf{x} \in \Gamma \tag{3.36}$$

which means that the pressure difference between inner and outer regions should be equal to 1. The result of numerical simulation is shown in Fig. 3.8 which denotes that the pressure jump at the interface is captured accurately.

Moreover, in order to verify surface tension force balance at the interface we use wobbling of an ellipse as a result of capillary forces to verify the solution of pressure equation. In this benchmark problem an elliptic droplet oscillates under the effect of

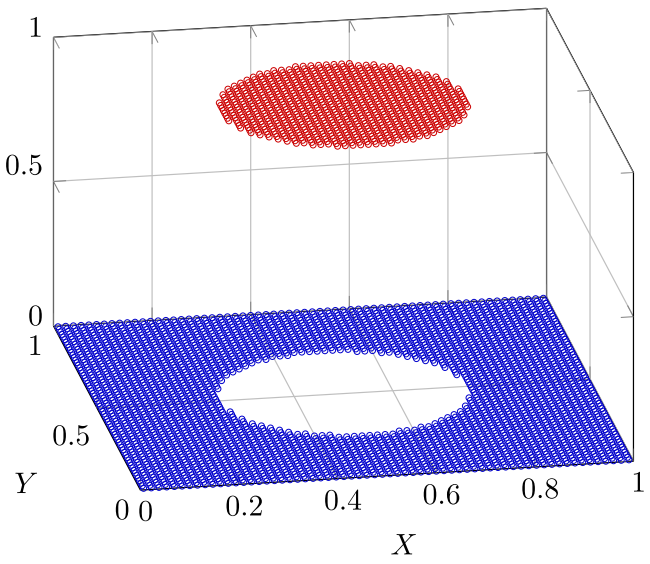


Figure 3.8: Results of Poisson equation with jump condition at the interface.

capillary forces. After a few oscillations the droplet reaches to an equilibrium condition with a circular interface. Ideally after reaching the equilibrium condition there should not exist any velocity field around the droplet. However, because of numerical errors there is small spurious current around the droplet finally after reaching the equilibrium condition. In this example the level set field is initialized using the equation,

$$\phi^0(x,y) = \left( \sqrt{\left( \frac{x^2}{2} + \frac{y^2}{1} \right)} - 0.25 \right), \tag{3.37}$$

We solve Navier-Stokes equations using the methodology described in Section. 2.3. We assumed $\sigma = 1$ and constant density and viscosities ($\rho = 1$, $\mu = 1$). The pressure jump at the interface induce a velocity field in the domain. Finally after several oscillations takes a circular shape with small spurious flows around it.

## 3.8 Imposing Constant Angle at Tri-Junction Point

Triple point in solidification of liquid droplet plays a critical role in formation of cusp on top of the droplet based on the theoretical and experimental studies (Marin et al. [12]). Moreover, the shape of the solidifying front depends on the angle at the tri-junction point. In experimental observations it is reported that the shape of interface can be changed from convex to concave in a droplet resting on a hydrophobic substrate. This

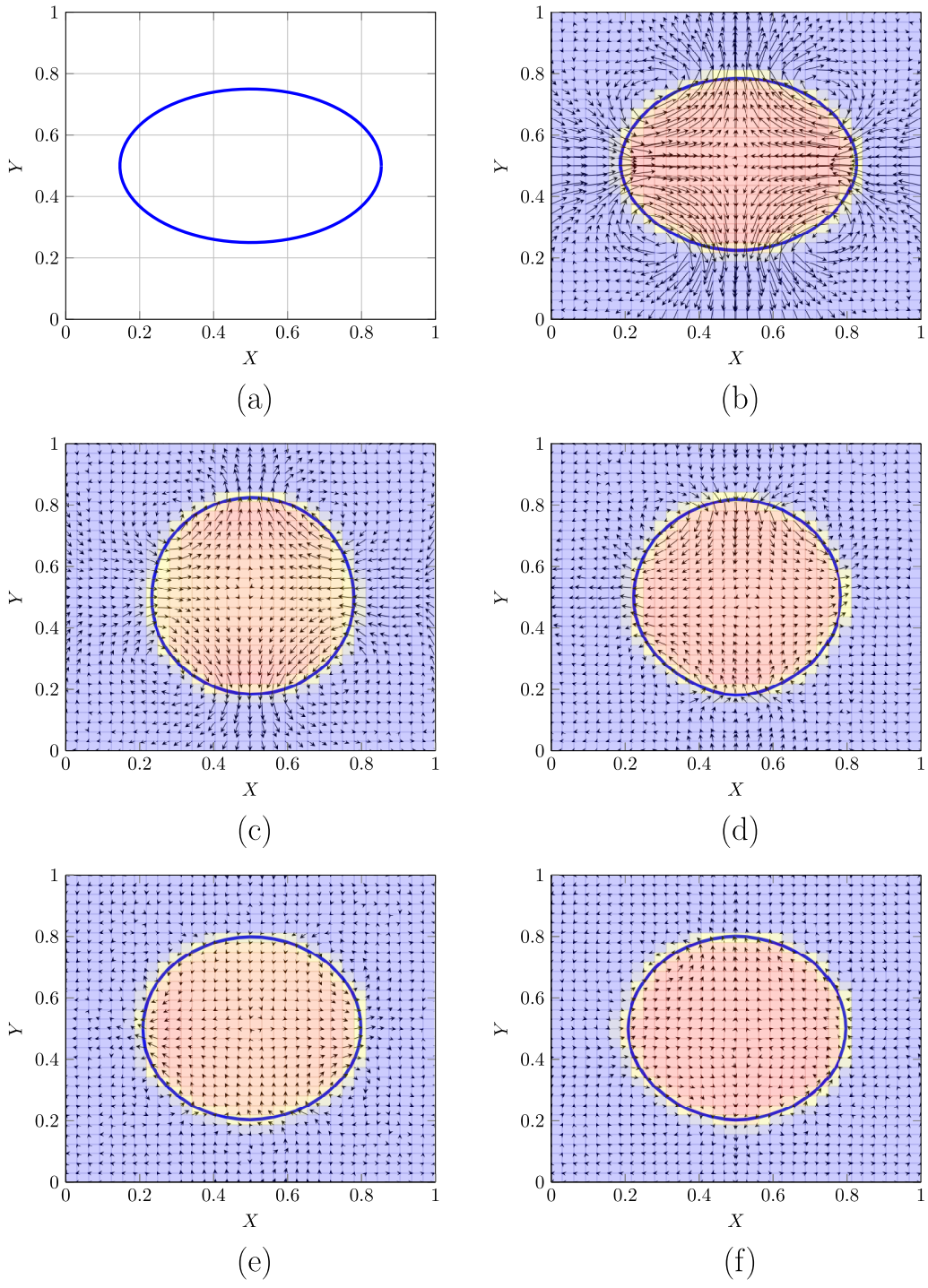


Figure 3.9: Results of oscillating elliptical droplet under effect of capillary forces after a)100 b) 200, c) 300, d) 400 iterations.

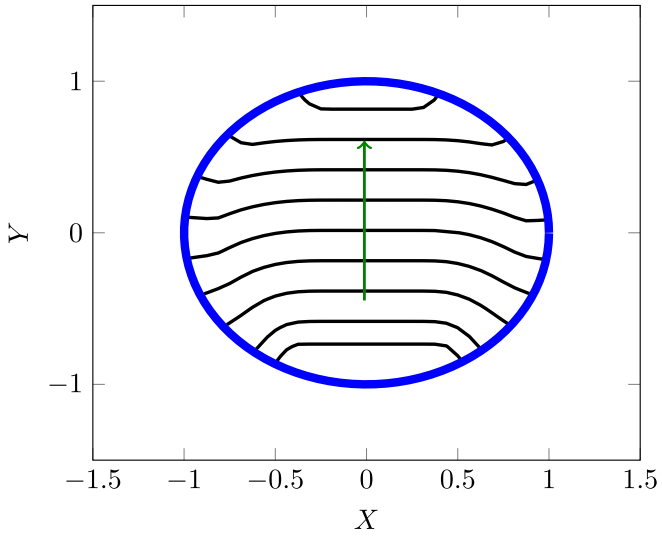


Figure 3.10: Imposing constant angle at the tri-junction point between two interfaces.

change of solidifying front is partially because of the angle at the tri-junction point. As explained in Section. 2.4.2 we solve a pseudo time dependent equation to reach steady state condition based on the predefined tolerance to impose the angle in the outer region of the droplet. Solving the equation in the outside will also affect the cells that are situated inside near the interface and inside the droplet.

In this section we use the method described in Section. 2.4.2 to impose a constant angle between two interfaces. Each interface is associates with a level-set. Initially we have a circle interface situated at the center of the domain. The second interface which is initially a straight line is moving from bottom to top of the circle with a constant velocity. Using the method described in Section.2.4.2 with the tolerance of $1 \times 10^{-4}$ as a criteria for reaching the steady-state condition, we impose a perpendicular angle at the tri-junction point. By solving the equation we impose the angle in cells situated near the interface. However, we use an offset of the circle interface to have the angle imposed inside the circle. Hence we define an auxiliary level-set field as,

$$\phi_{e_{i,j}} = \phi_{i,j} + \epsilon \tag{3.38}$$

where $\phi_e$ is the auxiliary level-sets which is used to impose the angle at the tri-junction point. We choose $\epsilon = \Delta x$ to have at least one grid cell between auxiliary and circle level-sets. As can be seen in Fig. 3.10 shape of the moving interface is changing from convex at the bottom of the circle to concave to top on the circle.

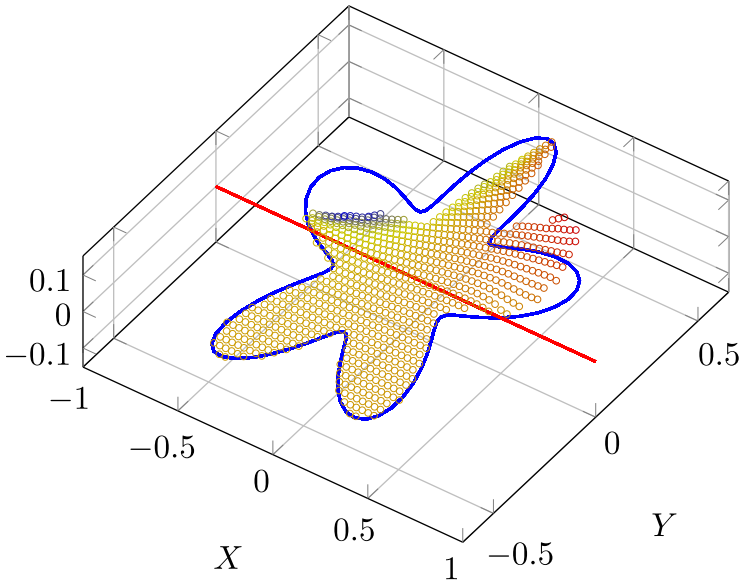


Figure 3.11: Solution of heat equation in a specific region where one of the level-sets is positive (solid red line) and the other one (star shape) is negative.

## 3.9 Multi-Region Heat Equation

In order to solve heat equation for solidifying droplet we need to divide computational domain into three regions. In this model, each region represents one phase and we should impose a constant temperature boundary condition on moving solidifying interface only inside the liquid region. To this end, we use two distinct level-sets to distinguish phases. Using the approach presented in Section. 2.4.3 we can solve heat equation only in one region without affecting the solution on the other side. In order to test the proposed approach we use the same problem presented in Section. 3.4 by including another level-set with a straight line interface to divide the star shape domain into two regions, namely active and passive. We wish to solve heat equation only in the active part where Dirichlet boundary condition is applied at the interface. In the passive part, on the other hand, we don't apply boundary conditions at the interface.

We use the sign of level-sets to determine where boundary conditions should be applied. The equation presented in Section. 3.5 are solved in the same star-shape domain. However, we divide the domain into two sections and only apply boundary conditions at the interface in the active segment. As can be seen in Fig. 3.11 the heat equation is only solved in the upper side of the red line while the other side is not affected by the heat equation.

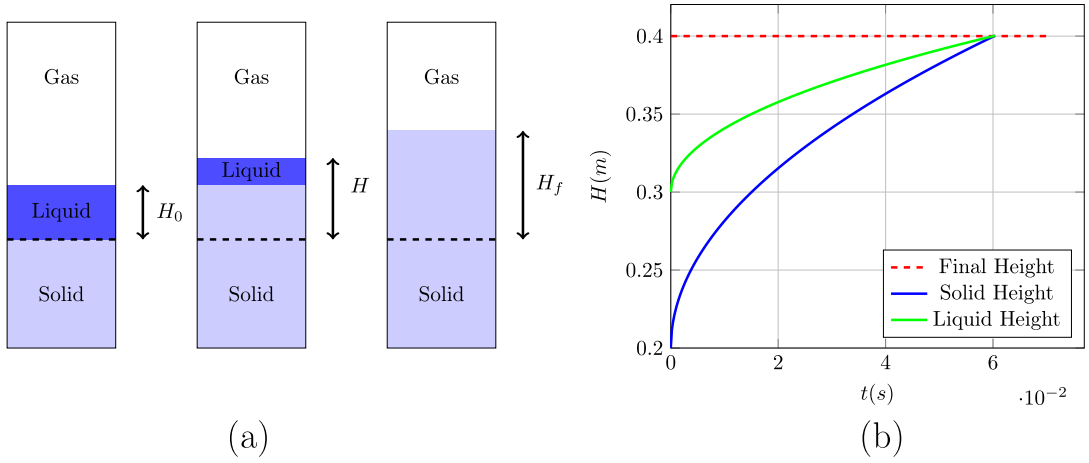


Figure 3.12: (a) Schematic of the three-phase Stefan problem. (b) Location of liquid and solid interfaces against time

## 3.10 Solidification of Liquid Column With Density Expansion

In order to accurately predict the behaviour of droplet freezing process we need to consider the density expansion of the liquid during phase change. In the three-phase solidification problem the solidifying interface and liquid interface should be coupled in some way. In the present study we include the effect of density expansion by coupling liquid and solid interfaces using a source term in the pressure correction step as described in Section. 2.4.5. In this approach the moving solidifying interface induces velocity field by which the liquid interface is evolved.

In order to validate the approach presented in Section.2.4.5 we simulate the density expansion of a liquid column. The schematic of problem is depicted in Fig. 3.12. In this problem we deal with liquid, gas, and solid phases. The liquid-solid phase is governed by the solidification rate and thermal properties of each phase. In this problem the liquid interface is initially located at height of $H_0$. After complete solidification the height of the solidified liquid is equal to $H_f$. We assume liquid is denser than the solid. Thus, from conservation of mass, the final height of the liquid slab $H_f$, can be obtained from

$$H_f = \frac{\rho_l}{\rho_s} H_0. \tag{3.39}$$

To simulate this problem using the proposed method, we use a $H_0 = 0.2m$ column of liquid exposed to cold surface. The solidifying front starts to move from bottom to top inducing velocity field in the liquid. Here we assume that the density ratio of liquid to solid is $\frac{\rho_l}{\rho_s} = 2$. Thus the final height of the liquid column should be $0.4m$. We use the

following relation to quantify the errors. The order of convergnece of liquid interface position prediction is affected by the order of accuracy of Stefan problem which is first order as can be seen in Table. 3.5.

$$E = \frac{|H_{Numerical} - H_{Exact}|}{H_{Exact}} \tag{3.40}$$

Table 3.5: Summary of errors of final solid height Stefan problem with density change

| Number of Cells | $L^1 - Error$ | Order |
|---|---|---|
| $32 \times 32$ | $4.3 \times 10^{-2}$ | - |
| $64 \times 64$ | $2.1 \times 10^{-2}$ | 1.0 |
| $128 \times 128$ | $1.0 \times 10^{-2}$ | 1.1 |

## 3.11 Solidification of Water Droplet

Water droplet freezing phenomenon involves various physical occurrences which should be considered at the same time in an accurate model. One of the most important aspects of a physical phenomenon is the time scale which should be considered in numerical investigations. There are three major physics in droplet freezing process: Surface tension; Density expansion; Solidification. Considering the surface tension forces the stability constraint can be expressed in the form of

$$\Delta t_\sigma < \sqrt{\frac{(\rho_l + \rho_g)\Delta x^3}{4\pi\sigma}}, \tag{3.41}$$

where $\rho_l$ and $\rho_g$ are densities of liquid and air. The physical explanation is that the time step should be small enough to resolve the fastest capillary waves in the system. A more detailed discussion about time constraints related to capillary forces can be found in the work of Popinet [49]. On the other hand, the time scale of the solidification is independent of the fluid flow and mainly depends on the thermal characteristics of the liquid and the solid. The total freezing time $t_f$ mainly depends on the $Ste$ number. As a result the mean velocity of the interface can be expressed as $u_{fm} = \lambda \frac{t_f}{R_0}$, where $\lambda$ is a constant and $R_0$ is droplet radius. The velocity induced by the density expansion can be expressed as $u_{exp} \propto \beta u_{fm}$ , where $\beta$ represents the expansion ratio and is less than one. As a result the velocity of the solidifying interface is larger than the velocity induced by the density expansion and can be used to obtain the maximum velocity in the domain. In numerical simulations the transport of the interface is subject to the standard CFL constraint $\Delta t_{adv} < \Delta x / |u_{fm}|$. Thus we can express the ratio of these two

stability constraints as

$$\frac{\Delta t_\sigma}{\Delta t_{adv}} = \sqrt{\frac{(\rho_l + \rho_g)|u_{fm}|^2 \Delta x}{4\pi\sigma}} = \sqrt{We_\Delta}, \tag{3.42}$$

where $We_\Delta$ is the cell Weber number, which represents the ratio of inertial to surface tension forces.

In the case of $600\mu m$ stationary water droplet freezing on a cold plate the freezing time is around $t_f = 30s$ based on the experimental studies in the literature which leads to a mean solidifying interface velocity of $u_{fm} = 20\mu m/s$. Thus the ratio two time constraints is,

$$\frac{\Delta t_\sigma}{\Delta t_{adv}} = \sqrt{We_\Delta} = \sqrt{We_R} N^{-1/2} \equiv 1 \times 10^{-5} N^{-1/2} \tag{3.43}$$

where $We_R$ is the droplet Weber number which is based on the droplet radius and mean solidifying interface velocity, and $N$ is the number of grid points per droplet radius. Hence, for a moderate resolution of $N = 10$, the capillary time step is $2 \times 10^6$ times smaller that the freezing time step. This stringent time step restriction leads to extremely high computational cost for fully resolved water droplet solidification process.

In addition to computational cost caused by capillary time steps, the numerical errors induced by each iteration is significant. One of the major sources of error in numerical simulation in the level-set method is re-initialization process. In each time step we need to re-initialize both droplet and the solidifying interfaces. These large number of re-initializations leads to significant mass loss and numerical noise in the calculation of the curvature which is discussed in du Chéné et al. [50].

In order to avoid the prohibitive time step constraint which is a cause of multi-physic nature of the droplet freezing we divide our numerical simulations into two parts. In the first part we neglect the density expansion focusing on the thermal behaviour of droplet during the freezing process of the droplet. Thermal properties of the droplet are assumed not to be affected by the fluid flow. In the second part, we will use a small number for the latent heat of fusion in order to have interface velocities at the same order of induced fluid velocity. With this assumption we will investigate the droplet shape change during the solidification. It is notable that all simulations in this section are performed on axisymmetric coordinates.

In order to verify how accurate the proposed model can predict the thermal behaviour of a freezing droplet we use the experimental results presented by Hu and Jin [14]. The none-dimensional parameters used to simulate the freezing process in this case are $Pr = 7.25$, $St = 0.025$, $\frac{k_s}{k_l} = 3.8$, $\frac{Cps}{Cpl} = 0.5$, $\frac{\rho_s}{\rho_l} = 1$. The required freezing time is the most important thermal characteristic of freezing droplets on cold substrates. The freezing time ($t_f$) is defined as the time interval required to have a droplet completely

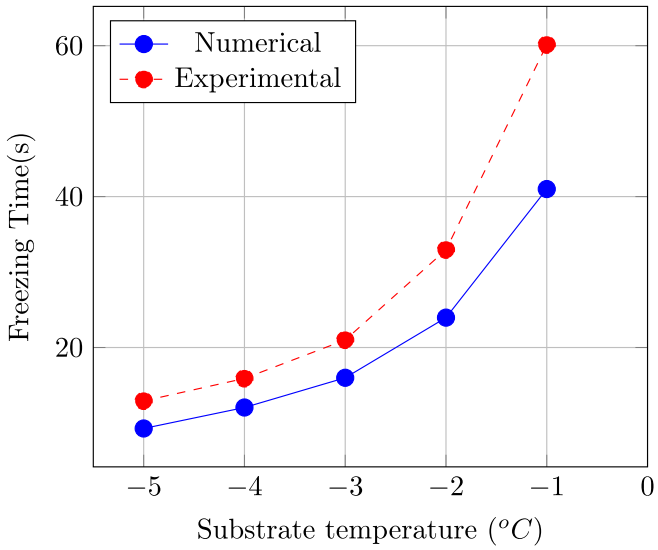


Figure 3.13: Comparison of predicted freezing time against experiments of Hu and Jin [14]

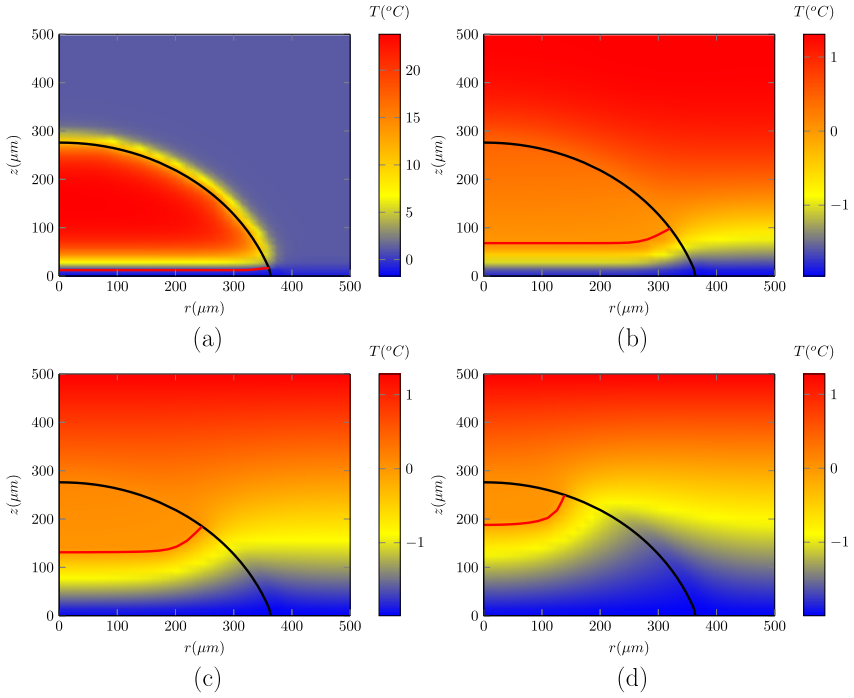


Figure 3.14: Freezing droplet temperature field at times a) $t = 0$, b) $t = 0.1t_f$, c) $t = 0.4t_f$, and d) $t = 0.7t_f$

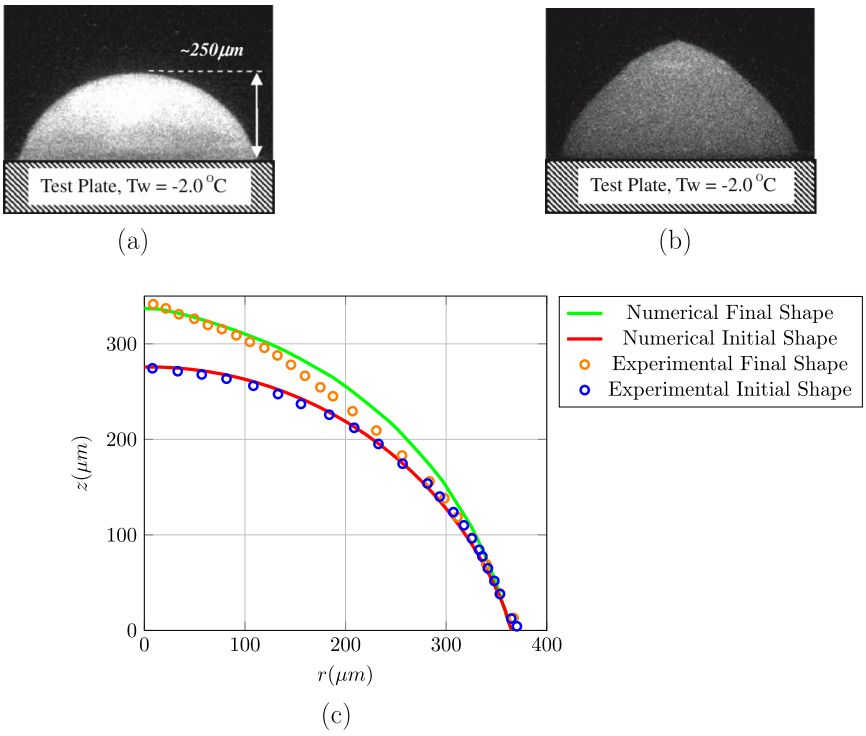


Figure 3.15: Comparison of numerical simulations against experimental results taken form Hu and Jin [14]. (a) initial droplet shape, (b) final droplet shape, (c) interface of droplet at initial and final stages of freezing process using experimental results of Hu and Jin [14] (symbols) and numerical simulations (solid lines)

turned to ice. The freezing time is of the great importance to aerospace industry since the required freezing time would determine the types of the ice formation on airplane wings.

In Fig. 3.13 the freezing time obtained from the proposed model is compared with those of presented by Hu and Jin [14] for a single droplet deposited on a cold plate for different substrate temperatures. In this test problem the grid is divided into 128 cells in each direction. The initial solidifying interface is a straight line above the substrate. As expected the freezing time decreases exponentially by decreasing the substrate temperature. Detailed temperature distribution in three phases is plotted in Fig.3.14. Note that temperature is fixed to zero at the droplet interface and the temperature at the air is not affected by ice level-set.

The difference between predicted and experimental freezing times is partially caused by numerical errors specially the errors in the re-initialization step. Since in each time step we impose the tri-junction angle the solidifying interface may artificially move. On the other hand, the average droplet temperature increases with time in spite of the fact that the freezing front is moving upward. This increase in the liquid temperature is presented by Hu and Jin [14]. They postulated that the release of latent heat of fusion

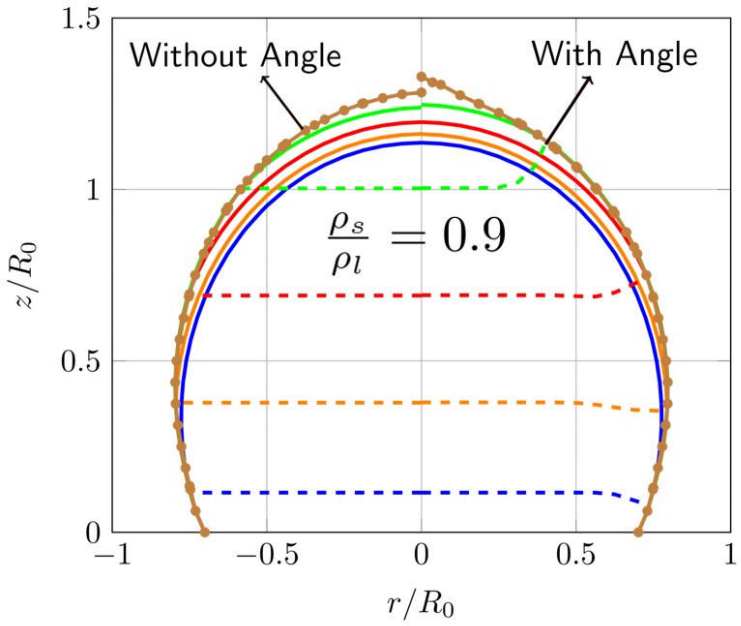


Figure 3.16: Droplet shape change for a stationary droplet on a hydrophobic cold substrate. Left: without imposing tri-junction angle; Right: with imposing tri-junction angle.

may be a cause of this temperature increase. However, as can be seen in Fig. 3.14 the temperature of the liquid part of the droplet is around $0^oC$ during the freezing process. Another reason for difference between numerical and experimental freezing time is that we neglected the effect of droplet shape change. In the case of expanding droplet the freezing time will increase by $10 - 30\%$ based on the numerical experiments.

In the next step in order to validate the accuracy of proposed approach for modelling density expansion we use a small latent heat of fusion ($St = 2.5 \times 10^3$). We also used the density ratio of $\frac{\rho_s}{\rho_l} = 0.9$. Result of stationary water droplet freezing on a cold substrate is presented in Fig. 3.15. We use the experimental result of Hu and Jin [14] to validate the proposed model. In the experiment a $500\mu m$ water droplet is deposited on a cold plate with the constant temperature of $-2^oC$. The computational domain is divided into 128 cells in each direction. Initial and final shapes of the droplet are compared with the experimental observations in Fig. 3.15. As can be seen the presented level-set based model is capable of accurately predicting the cusp formation on top of the droplet.

Even though the formation of pointy cone on top of the droplet has been attributed to the expansion of water upon freezing, there is still little explanation for this phenomenon in the literature. Marin et al. [12] postulated that the pointy shape is because of tri-junction angle. In Fig. 3.16 the result of droplet shape is plotted in different times. In the left side we didn't impose the tri-junction angle while in the right side we impose $90^o$ tri-junction angle. As can be seen the pointy shape is formed in the case of imposing

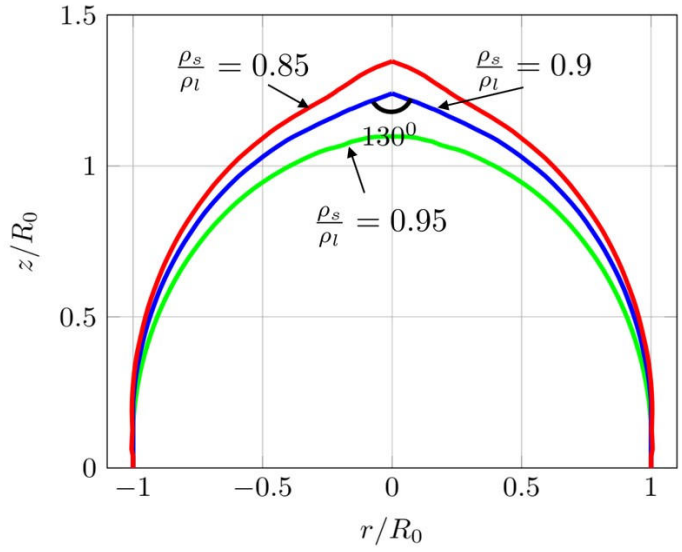


Figure 3.17: Effect of solid to liquid density ratio on protrusion formation on top of freezing droplet. Red, Blue, and Green lines are associated with 0.85, 0.9, and 0.95 solid to liquid density ratios, respectively.

constant tri-junction angle. Hence, we can conclude that the formation of pointy shape on top of freezing droplets is a result of density expansion and fixed tri-junction angle.

It has been known that formation of protrusion on the of water droplets is mainly because of volume expansion. In order to investigate effect of solid to liquid density ratio we modelled droplet freezing with different density ratios. As can be seen in Fig. 3.17 the density ratio of ice to water should not be larger than 0.9 to have protrusion formed. For larger density ratios the pointy cone will not be formed. Furthermore the angle of protrusion for the case of $\rho_s/\rho_l = 0.9$ is measure to be $130^0$ which is in the range of reported measurements of Marin et al. [12] which is between $130^0$ and $145^0$. Numerical results indicate that decreasing the density ratio of solid to liquid will lead to large droplet deformation and smaller cone angle.

# Chapter 4

# Conclusions

The main aim of this thesis was to extend the level-set method for numerically modelling of water droplet freezing process. The proposed model is generally capable of modelling solidification of liquids in the presence of three phases. In particular we used the model for simulation of a stationary water droplet on a cold plate.

We used two distinct level-sets to represent the liquid-solid and liquid-gas interfaces. The liquid-solid interface is governed by heat transfer equations while the liquid-gas interface is governed by Navier-Stokes equations. Generally we need to deal with three different discontinuities at liquid-solid and liquid-gas interfaces. We used the ghost cell approach to set boundary conditions at the moving interface and deal with the temperature discontinuity. In addition, the latent heat of fusion is included in the calculation of solidification speed.

The level-set associated with the solidifying interface is divided into two segments, namely: active and passive. The active part is governed by heat transfer in the liquid while the passive part is used to impose a constant angle at the tri-junction point. In order to impose the angle at the tri-junction point we proposed a pseudo-time dependent equation which should be solved to reach steady state conditions. By solving the proposed transient equation we moved only the passive part while the active part is held fixed.

We solved Navier-Stokes equations using second order spatial and temporal schemes. In order to impose pressure jump condition at the liquid-air interface we used the ghost fluid method. Density expansion due to phase change is included in the proposed model using a source term in continuity equation. The density expansion appears as a source term creating a high pressure zone at the solidifying front. The high pressure zone induces velocity in the domain by which the droplet interface is advected.

The numerical model was validated using experimental results in the literature. Through the comparison the effect of density expansion on the final droplet shape and cusp formation on top of droplet was investigated. Comparing the numerical results against experimental images suggested that the proposed level-set approach

can accurately predict the behavior of solidifying process. The most significant aspects of this study can be summarized as follows.

- Extended level-set approach to model three-phase unconstrained solidification process.
- Extended the ghost cell approach to impose fixed value boundary condition on moving solidifying front only inside the liquid.
- Proposed an equation for imposing constant angle at the tri-junction point.
- Modified pressure correction equation to include density expansion.
- Modified level-set equation to impose conservation of mass in the liquid part.
- Considered effect of density expansion in energy equation which is neglected in the literature.

The proposed model makes it possible to numerically study a wide range of physical phenomena which was not feasible before. In the following a few physical occurrences that can be modelled by the proposed approach are presented.

- Water droplet freezing on cold plates in room temperature.
- Super cooled water droplet freezing process.
- Solidification of pure materials in the presence of three phases.
- Freezing of liquid film layer on flat surfaces, airfoils or any complicated geometries.
- Freezing of liquids in open containers.

## 4.1 Computational Challenges

As mentioned before the proposed model is capable of modelling three-phase solidification process. However, there are some numerical challenges which will be reviewed in this section.

Level-set methods are generally known to suffer from mass loss. We used second-order ENO scheme to alleviate the mass loss in advection equation. However, during the re-initialization process we may loss mass because of numerical errors. There are various remedies to reduce the mass loss during the re-initialization process such as particle level-set method. It can be useful to incorporate those methods in solidification problems.

Since in the droplet solidification problem a variety of physics are involved the time step restrictions are extremely stringent. As a result, the computational cost of refined grids is high. Therefore, numerical improvements are required in this part to avoid prohibitively small time steps.

Generally in multiphase problems we are only interested in having refined grids at the interfaces. In other parts of the domain we can use coarser grids. As a result, utilization of adaptive grid refinement strategies is useful in three phase solidification problems.

The numerical model is developed for two dimension problems while extending the problem into three-dimension is straight forward in a dimension by dimension manner. However, computational cost of three dimensional simulations are high and parallel computational techniques should be employed to improve the speed of computations.

## 4.2 Future Works

Detailed numerical simulation of solidification problems require more improvements in the level-set framework. Some possible improvements are outlined in this section. The approach presented in this study is useful for modelling solidification of stationary droplets. In order to model dynamics of impacting droplets the model requires further improvements. The incipient of ice formation at the contact line of the droplet and the substrate requires special treatment. A possible approach is to use temperature field at the beginning of the solidification and construct level-sets from the temperature field.

In experiments of Hu and Jin [14] it has been observed that the temperature of the liquid portion is increasing over time ($10^o$) while in the current state of mathematical description of solidification process the temperature of the liquid part decreases as a result of heat transfer to the ambient and to the substrate. The increase in the liquid portion of the droplet should be modelled mathematically.

In the current model we used source term at the solidification interface to induce velocity in the field as a result of density expansion. However, the source term approach may be replaced by more accurate approaches similar to ghost fluid method to directly induce velocity in liquid.

# Bibliography


[1] M. Bragg, Aerodynamics of supercooled-large-droplet ice accretions and the effect on aircraft control, in: Proceedings of the FAA International Conference on Aircraft Inflight Icing, vol. 2, 387–399, 1996.

[2] T. Vu, G. Tryggason, S. Homma, J. Wells, H. Takakura, Front Tracking Computation of Trijunction Solidification with Volume Change, Procedia IUTAM 15 (2015) 14–17.

[3] J. Madejski, Solidification of droplets on a cold surface, International Journal of Heat and Mass Transfer 19 (9) (1976) 1009–1013.

[4] T. Bennett, D. Poulikakos, Heat transfer aspects of splat-quench solidification: modelling and experiment, Journal of Materials Science 29 (8) (1994) 2025–2039.

[5] B. Kang, Z. Zhao, D. Poulikakos, Solidification of liquid metal droplets impacting sequentially on a solid surface, Journal of Heat Transfer 116 (2) (1994) 436–445.

[6] M. Pasandideh-Fard, R. Bhola, S. Chandra, J. Mostaghimi, Deposition of tin droplets on a steel plate: simulations and experiments, International Journal of Heat and Mass Transfer 41 (19) (1998) 2929–2945.

[7] M. Fukumoto, Y. Huang, Flattening mechanism in thermal sprayed nickel particle impinging on flat substrate surface, Journal of Thermal Spray Technology 8 (3) (1999) 427–432.

[8] R. Bhola, S. Chandra, Parameters controlling solidification of molten wax droplets falling on a solid surface, Journal of materials science 34 (19) (1999) 4883–4894.

[9] D. Attinger, Z. Zhao, D. Poulikakos, An experimental study of molten microdroplet surface deposition and solidification: transient behavior and wetting angle dynamics, Journal of Heat Transfer 122 (3) (2000) 544–556.

[10] J. Hindmarsh, A. Russell, X. Chen, Experimental and numerical analysis of the temperature transition of a suspended freezing water droplet, International Journal of Heat and Mass Transfer 46 (7) (2003) 1199–1213.

[11] J. Wang, Z. Liu, Y. Gou, X. Zhang, S. Cheng, Deformation of freezing water droplets on a cold copper surface, Science in China Series E: Technological Sciences 49 (5) (2006) 590–600.

[12] A. G. Marin, O. R. Enriquez, P. Brunet, P. Colinet, J. H. Snoeijer, Universality of tip singularity formation in freezing water drops, Physical review letters 113 (5) (2014) 054301.

[13] Z. Jin, Q. Dong, S. Jin, Z. Yang, Visualization of the freezing and melting process of a small water droplet on a cold surface, in: International Conference on Fluid Dynamics and Thermodynamics Technologies, vol. 3, 125–129, 2012.

[14] H. Hu, Z. Jin, An icing physics study by using lifetime-based molecular tagging thermometry technique, International Journal of Multiphase Flow 36 (8) (2010) 672–681.

[15] P. Tourkine, M. Le Merrer, D. Quéré, Delayed freezing on water repellent materials, Langmuir 25 (13) (2009) 7214–7216.

[16] D. P. Singh, J. P. Singh, Delayed freezing of water droplet on silver nanocolumnar thin film, Applied Physics Letters 102 (24) (2013) 243112.

[17] L. Huang, Z. Liu, Y. Liu, Y. Gou, L. Wang, Effect of contact angle on water droplet freezing process on a cold flat surface, Experimental thermal and fluid science 40 (2012) 74–80.

[18] S. Jung, M. K. Tiwari, N. V. Doan, D. Poulikakos, Mechanism of supercooled droplet freezing on surfaces, Nature communications 3 (2012) 615.

[19] G. Chaudhary, R. Li, Freezing of water droplets on solid surfaces: An experimental and numerical study, Experimental Thermal and Fluid Science 57 (2014) 86–93.

[20] V. Voller, Implicit finite difference solutions of the enthalpy formulation of Stefan problems, IMA journal of numerical analysis 5 (2) (1985) 201–214.

[21] H. Hashemi, C. Sliepcevich, A numerical method for solving two-dimensional problems of heat conduction with change of phase, in: Chem. Eng. Prog. Symp. Series, vol. 63, 34–41, 1967.

[22] D. Poirier, M. Salcudean, On numerical methods used in mathematical modeling of phase change in liquid metals, Journal of heat transfer 110 (3) (1988) 562–570.

[23] V. Voller, M. Cross, An explicit numerical method to track a moving phase change front 26 (1) (1983) 147–150.

[24] V. Voller, N. Markatos, M. Cross, Techniques for accounting for the moving interface in convection/diffusion phase change., Pineridge Press, 1985.

[25] F. Rösler, D. Brüggemann, Shell-and-tube type latent heat thermal energy storage: numerical analysis and comparison with experiments, Heat and mass transfer 47 (8) (2011) 1027.

[26] Y. Cao, A. Faghri, W. S. Chang, A numerical analysis of Stefan problems for generalized multi-dimensional phase-change structures using the enthalpy transforming model, International journal of heat and mass transfer 32 (7) (1989) 1289–1298.

[27] M. Pasandideh-Fard, S. Chandra, J. Mostaghimi, A three-dimensional model of droplet impact and solidification, International Journal of Heat and Mass Transfer 45 (11) (2002) 2229–2242.

[28] M. Raessi, J. Mostaghimi, Three-dimensional modelling of density variation due to phase change in complex free surface flows, Numerical Heat Transfer, Part B: Fundamentals 47 (6) (2005) 507–531.

[29] S. O. Unverdi, G. Tryggvason, A front-tracking method for viscous, incompressible, multi-fluid flows, Journal of computational physics 100 (1) (1992) 25–37.

[30] D. Juric, G. Tryggvason, A front-tracking method for dendritic solidification, Journal of computational physics 123 (1) (1996) 127–148.

[31] V. Alexiades, Mathematical modeling of melting and freezing processes, Routledge, 2017.

[32] B. Merriman, J. K. Bence, S. J. Osher, Motion of multiple junctions: A level set approach, Journal of Computational Physics 112 (2) (1994) 334–363.

[33] S. Osher, R. Fedkiw, Level set methods and dynamic implicit surfaces, vol. 153, Springer Science & Business Media, 2006.

[34] F. Gibou, R. Fedkiw, R. Caflisch, S. Osher, A level set approach for the numerical simulation of dendritic growth, Journal of Scientific Computing 19 (1-3) (2003) 183–199.

[35] M. Bussmann, J. Mostaghimi, S. Chandra, On a three-dimensional volume tracking model of droplet impact, Physics of Fluids 11 (6) (1999) 1406–1417.

[36] M. Pasandideh-Fard, Droplet impact and solidification in a thermal spray process, Ph.D. thesis, National Library of Canada= Bibliothèque nationale du Canada, 1999.

[37] N. Al-Rawahi, G. Tryggvason, Numerical simulation of dendritic solidification with convection: two-dimensional geometry, Journal of Computational Physics 180 (2) (2002) 471–496.

[38] M. Sussman, P. Smereka, S. Osher, A level set approach for computing solutions to incompressible two-phase flow, Journal of Computational physics 114 (1) (1994) 146–159.

[39] C.-W. Shu, S. Osher, Efficient implementation of essentially non-oscillatory shock-capturing schemes, Journal of computational physics 77 (2) (1988) 439–471.

[40] C. Min, On reinitializing level set functions, Journal of computational physics 229 (8) (2010) 2764–2772.

[41] F. Gibou, R. Fedkiw, L. Cheng, M. Kang, A second-order-accurate symmetric discretization of the Poisson equation on irregular domains, Journal of Computational Physics 176 (1) (2002) 205–227.

[42] D. Adalsteinsson, J. A. Sethian, The fast construction of extension velocities in level set methods, Journal of Computational Physics 148 (1) (1999) 2–22.

[43] A. J. Chorin, On the convergence of discrete approximations to the Navier-Stokes equations, Mathematics of computation 23 (106) (1969) 341–353.

[44] J. B. Bell, P. Colella, H. M. Glaz, A second-order projection method for the incompressible Navier-Stokes equations, Journal of Computational Physics 85 (2) (1989) 257–283.

[45] R. Fedkiw, T. Aslam, B. Merriman, S. Osher, A non-oscillatory Eulerian approach to interfaces in multimaterial flows (the ghost fluid method), Journal of computational physics 152 (2) (1999) 457–492.

[46] G. Russo, P. Smereka, A remark on computing distance functions, Journal of Computational Physics 163 (1) (2000) 51–67.

[47] M. Rudman, Volume-tracking methods for interfacial flow calculations, International journal for numerical methods in fluids 24 (7) (1997) 671–691.

[48] M. Sussman, E. Fatemi, An efficient, interface-preserving level set redistancing algorithm and its application to interfacial incompressible fluid flow, SIAM Journal on scientific computing 20 (4) (1999) 1165–1191.

[49] S. Popinet, Numerical models of surface tension, Annual Review of Fluid Mechanics 50 (2018) 49–75.

[50] A. du Chéné, C. Min, F. Gibou, Second-order accurate computation of curvatures in a level set framework using novel high-order reinitialization schemes, Journal of Scientific Computing 35 (2-3) (2008) 114–131.